Title
Monolithically Integrated Time-varying Transmission Line (TVTL) for Signal Processing

Author
Wu, Qianteng

Publication Date
2019

Peer reviewed|Thesis/dissertation

UNIVERSITY OF CALIFORNIA

Los Angeles

Monolithically Integrated Time-varying Transmission Line (TVTL) for Signal Processing

A dissertation submitted in partial satisfaction

of the requirements for the degree

Doctor of Philosophy in Electrical and Computer Engineering

by

Qianteng Wu

2019

ABSTRACT OF THE DISSERTATION

Monolithically Integrated Time-varying Transmission Line (TVTL)

for Signal Processing

by

Qianteng Wu

Doctor of Philosophy in Electrical and Computer Engineering

University of California, Los Angeles, 2019

Professor Yuanxun Wang, Chair

In-band jammer/interference that cannot be isolated by a filter in today's RF system could easily desensitize and saturate RF front-end. Performing signal processing directly at the RF front-end could reduce the in-band jammer/interference prior to the receiver to prevent the jamming, which enables the RF system has the ability to operate in the unpredicted and high interference environments. However, implementation of the signal processing block at the RF domain is usually challenging due to the insertion loss and noise introduced through the RF signal processing device could significantly degrade sensitivity and dynamic range of the receiver. Time-varying transmission line (TVTL), a novel RF circuit, which is time-varying capacitance periodically loaded on a transmission line, provides unique properties of low noise, low loss frequency conversion, broadband, and high power handling capability, provides a new solution enabling the RF signal processing at the RF front end. Meanwhile, the TVTL circuit can

be integrated into the modern Monolithic Microwave Integrated Circuit (MMIC) technology, which offers small physical dimensions and has the compatibility with other circuit blocks.

In this thesis, TVTL's theory and implementation are first introduced and studied. M-derived TVTL is designed and fabricated on MMIC and two types of correlators, open loop correlator, and closed loop correlator, based on the TVTL are studied, implemented and verified. Both frequency domain correlation tests and time domain decoder tests are carried out to validate the designed correlators. At the last, two advanced TVTL structures are proposed for the purpose of improving the power efficiency and conversion gain.

The dissertation of Qianteng Wu is approved.

Tatsuo Itoh

Benjamin S Williams

Troy A Carter

Yuanxun Wang, Committee Chair

University of California, Los Angeles

2019

This dissertation is dedicated to my family,

for their unconditional love, encouragement, and support.

TABLE OF CONTENTS

LIST OF FIGURES

SYMBOLS AND ACRONYMS

SNR	Signal-to-noise Ratio
RF	Radio Frequency
TVTL	Time-varying Transmission Line
FDD	Frequency Division Duplex
STAR	Simultaneous Transmit and Receive
CR	Cognitive Radio
DSSS	Direct Sequence Spread Spectrum
TX	Transmitter
RX	Receiver
DSP	Digital Signal Processing
PCB	Printed Circuit Broad
MMIC	Monolithic Microwave Integrated Circuit
NLTL	Nonlinear Transmission Line
Q	Quality Factor
NF	Noise Figure
LNA	Low Noise Amplifier
PA	Power Amplifier
3-D	Three-dimensional
HEMT	High-electron-mobility Transistor
HBT	Heterojunction Bipolar Transistor
BASK	Binary Amplitude Shifting Keying

BPSK	Binary Phase Shifting Keying
BFSK	Binary Frequency Shifting Keying

ACKNOWLEDGEMENTS

It has been a wonderful journey for both studying and working in Digital Microwave Lab at UCLA. First, I would like to give my special thanks to my advisor Professor Ethan Wang who lends to the world of the RF/microwave and time-varying circuit. With his continuous support and guidance, I gained a deep understanding and insight of not only the circuit itself but the physics behind it as well.

I would also like to acknowledge my doctoral committee members Professor Tatsuo Itoh, Professor Benjamin Williams and Professor Troy Carter for their advice and comments to help me to improve my work.

My project is deeply based on solid collaboration with my colleges and others. I would like to thank Xiating Zou and Dr. Lap K Yeung for their tight collaboration and Dr. Shihan Qin for his prior work on time-varying transmission line. I would also like to thank Dr. Qiang Xu, Dr. Rui Zhu, Dr. Yaozhong Liu, Dr. Zhi Yao, Dr. Mathew Biedka, Ting Lu and Dr. Cui Han for their inspiring and technical discussions on different fields, such as signal processing and electromagnetic.

I would like to thank Minji Zhu, the lab manager of the Center for High Frequency Electronics (CHFE) at UCLA, for his testing guide and support.

I would like to thank Michael Foster and Gary Ray from Boeing Research & Technology for their technical and programmatic discussions.

I also gratefully for the financial support for this work from the DARPA MTO SPAR Program.

I would like to thank Dr. Jinxi Guo, Chi Huang and Ziyue Chen for their supports and friendship.

Finally, I express my deepest love and special gratitude to my family for their unconditional love, encouragement and support.

VITA

Education

2015-2019 ***Graduate Student*** in **Electrical and Computer Engineering**
University of California, Los Angeles, USA

2013-2015 ***M.S.*** in **Electrical Engineering**
University of California, Davis, USA

2009-2013 ***B.S.*** in **Communication Engineering**
Hangzhou Dianzi University, Hangzhou, P. R. China

Publications

[1] **Q. Wu**, X. Zou, R. Zhu and Y. E. Wang, "Chip-Scale RF Correlator with Monolithically Integrated Time-Varying Transmission Line (TVTL)" in 2018 IEEE MTT-S Int. Microw. Symp. Philadelphia, PA, USA, June 2018.

[2] **Q. Wu**, X. Zou, S. Qin and Y. E. Wang, "Frequency Translational RF Receiver with Time Varying Transmission Lines" in 2017 IEEE MTT-S Int. Microw. Symp. Honolulu, HI, USA, June 2017, pp. 1767–1769.

[3] **Q. Wu**, X. Liu, "A 3.4-3.6 GHz High Efficiency Power Amplifier Using Bandpass Output Matching Network" in 2015 IEEE MTT-S Int. Microw. Symp. Phoenix, AZ, USA, May 2015, pp. ISBN 978-1-4799-8275-2.

Chapter 1

Introduction

The complicated EM environment in today's wireless system imposes great challenges for designing RF receivers. Sensitivity and dynamic range of the RF front-end could be significantly degraded when the RF receiver is exposed in unpredicted or unregulated EM environments as in-band jammer and interference cannot be filtered out. This issue can be solved by performing RF signal processing like correlation at the RF front-end as the spread spectrum system, such as the direct sequence spread spectrum (DSSS) system [1, 2], provides high processing gain, which enables the system to be immune to large interferences. Recently, the time-varying transmission line (TVTL) [3, 4, 5] is proposed, which carries properties such as broadband and low noise non-reciprocal frequency conversion, parametric amplification [6]. These properties make TVTL very suitable to work at the RF front-end [7, 8, 9, 10] and to realize complex signal processing functions, such as correlation directly at the RF domain [11].

1.1 Overview of Wireless System

Commercial systems usually use Frequency-division duplex (FDD) to separate receiver (RX) and transmitter (TX) as shown in Figure 1.1-1 and make carefully control and planning through standards, like cellular networks, to avoid in-band interference. Thus advanced digital signal processing could be employed in the baseband domain for performing complex algorithms, such as sorting out users and demodulate signals. In the unplanned and uncontrolled EM environment, in-band jammer and interference that cannot be blocked out by filter could easily

saturate and desensitize RF front-end, break down the signal-to-noise ratio (SNR) of the received signal and dynamic range of the receiver, which causes receiving failure.

To protect the receiver, received signals should be interrogated prior to the receiver as indicated in Figure 1.1-2, so signal processing in the RF domain is desired and necessary. In [12, 13, 14, 15], the N-path mixer is served as the first stage to reject the blocker. In [16, 17], interference is rejected by employed a positive feedback. By using the orthogonal codes and performing correlation at the RF domain, unwanted interference rejection and extra isolation from TX to RX could be obtained. Also, by using a correlator or mixer as the first stage in the receiver, local oscillation frequency could be changed to the desired band accordingly, thus this configuration could be used in software-defined radio (SDR) or cognitive radio (CR).

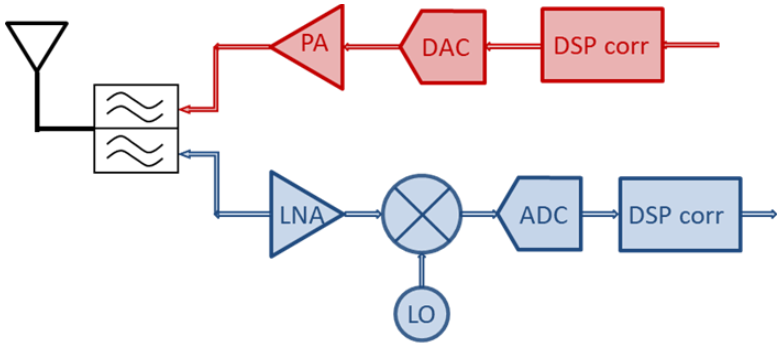

Figure 1.1-1. Scheme for duplex the RF signal by using the diplexer.

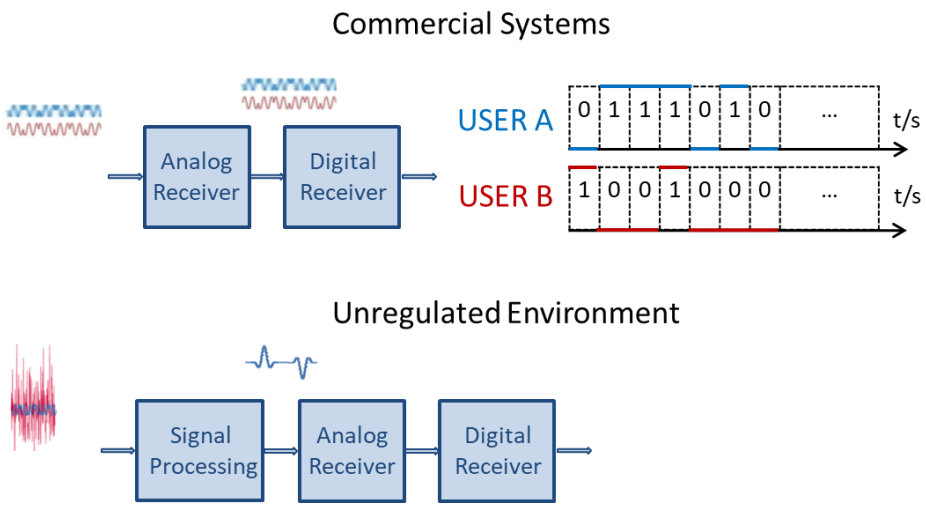

Figure 1.1-2. Commercial systems vs. unregulated environment systems.

A simultaneous transmit and receive (STAR) RF front-end architecture is proposed [18] for the receiver working in the unpredicted environment and enabling the transmitting and receiving at the same time is shown in Figure 1.1-3. TX correlator and RX correlator works as an RF encoder and decoder that reject the interference by using the orthogonal codes. Also, in this configuration, the circulator [19] [20] and RF correlator [9] [11] [21] could implemented by using the TVTL based components because of its unique properties, low loss, broadband, and low noise, the entire system could be benefited.

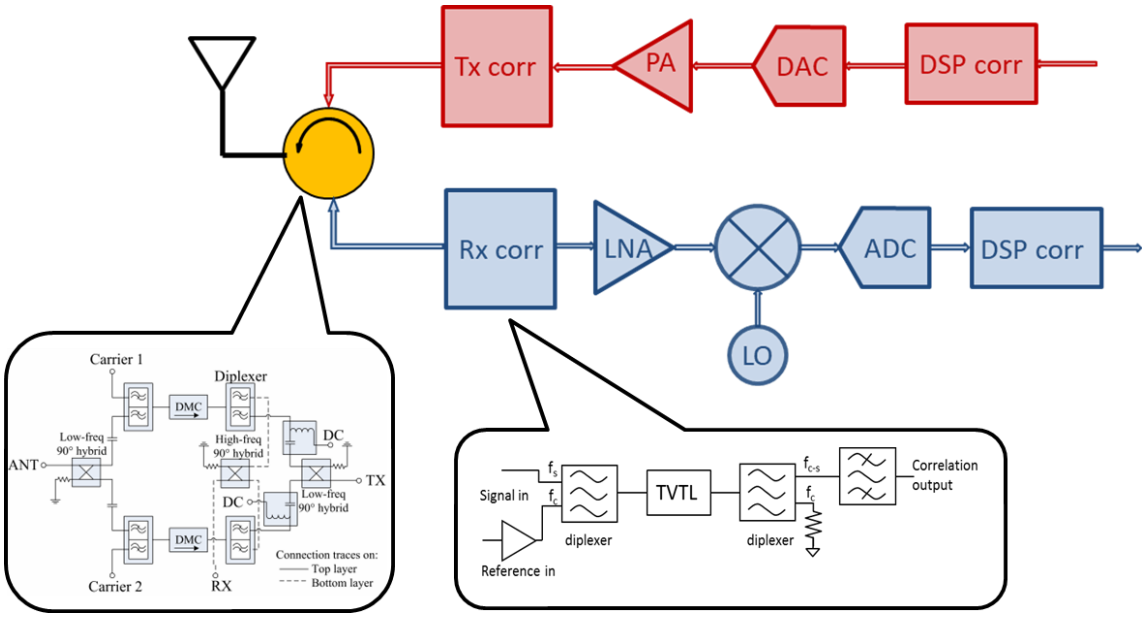

Figure 1.1-3. RF system with signal processing at the RF domain.

1.2 Time-varying Electromagnetic Devices

The time-varying electromagnetic device is formed when part of the boundary condition becomes time-varying. The fast varying impedance of semiconductor or electromechanical devices in a microwave structure forms an interesting class of time-varying electromagnetic devices. The time-varying circuit is in the middle of the active circuit and the passive circuit which is capable of avoiding the noise, power handling and power consumption issues associated with active transistor-based circuits while retaining the phase stability of in a typical structure. The time-varying operations are often introduced through the time-varying transmission line (TVTL).

1.3 Dissertation Outline

In this discussion, the time-varying transmission line's theory is first introduced in chapter 2, which includes parametric conversion gain and noise figure derivations. Meanwhile, TVTL's design procedure and implementation are presented, including both PCB and MMIC designs, which verifies the TVTL theory. In chapter 3, two correlators, open loop correlator and closed loop correlator, are designed and discussed in the perspectives of the operating principle, bandwidth and noise performance. And these two proposed correlators are validated by various tests including the frequency response, noise figure, correlation test, etc. and a brief comparison between two correlators is presented. Finally, in chapter 4, two advanced TVTL structures are introduced, which helps to lower the power consumption and boost the conversion gain.

Chapter 2

Basic of Time-varying Transmission Line and Its Implementation

Time-varying transmission line (TVTL) was first explored by P.K. Tien in 1958 [22, 23] and proved can be used for parametric amplification [24] and frequency mixing [25, 26] with intrinsic low noise [27, 28, 29]. The name of the TVTL should be differentiated with the classic nonlinear transmission line (NLTL) [30, 31] which finds its applications in pulse shaping, like pulse narrowing and pulse sharpening, and harmonic generating because of its favorable properties. The main difference between the TVTL and NLTL is that TVTL works in the linear region with limited bandwidth and variation is controlled by a carrier pump but NLTL only works for a large single tone or pulse.

2.1 Time-varying Transmission Line Theory

Figure 2.1-1. shows the lumped-element model of the time-varying transmission line, it is the same with the conventional transmission line but with time-varying capacitance. The distributed inductance L' is represented by a series inductor and capacitance $C'(z,t)$ varying as a function of time and space is represented by a shunt capacitor. This lossless lumped-element model consists of an infinite series of the infinitesimal elements shown in Figure 2.1-1, and the value of the components are specified per unit length.

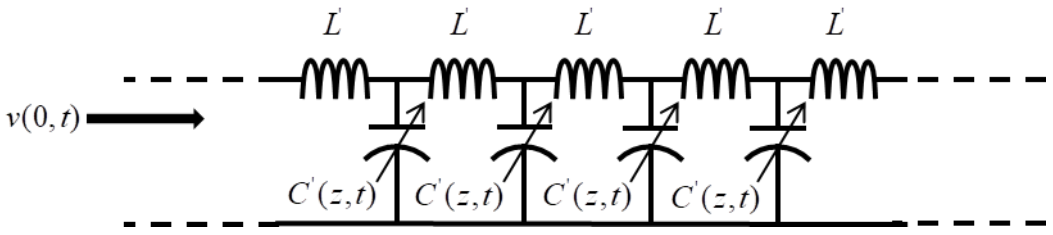

Figure 2.1-1. Lumped-element model of the time-varying transmission line with time-varying capacitance.

Applying the telegrapher's equations, thus can have:

$$\begin{cases} \frac{\partial v(z,t)}{\partial z} = -L' \frac{\partial i(z,t)}{\partial t} \\ \frac{\partial i(z,t)}{\partial z} = -\frac{\partial [C'(z,t) \cdot v(z,t)]}{\partial t} \end{cases} \tag{2.1-1}$$

Rearranging the equation of Eq. (2.1-1), Eq. (2.1-2) could be obtained.

$$\frac{\partial^2 v(z,t)}{\partial z^2} = L' \frac{\partial^2 [C'(z,t) \cdot v(z,t)]}{\partial t^2} \tag{2.1-2}$$

In the lumped-element infinitely long TVTL model, the capacitance per unit length is assumed to be modulated linearly by the voltage v_c across it and the variation of the capacitance can be expressed as:

$$C(v_c) = C_0 + C_1 \cdot v_c \tag{2.1-3}$$

Where the C_0 is the mean capacitance per unit length, C_1 is the linear capacitance variation versus the voltage per unit length. Usually, linear capacitance variation cannot be acquired in practice, but the mean capacitance and the first capacitance variation coefficient could be calculated by performing Fourier Series as these time-varying capacitance are usually modulated by a single tone carrier, a periodic signal. The first two coefficients are shown in Eq. (2.1-4):

$$\begin{cases} C_0 = \frac{1}{2\pi} \int_{-\pi}^{\pi} C(V_b + V_p \cdot cos\omega_c t) \cdot d\omega_c t \\ C_1 = \frac{1}{\pi} \int_{-\pi}^{\pi} C(V_b + V_p \cdot cos\omega_c t) \cdot cos\omega_c t \cdot d\omega_c t \end{cases} \tag{2.1-4}$$

Where the V_b is the biasing voltage and V_p is the amplitude of the modulation signal with a frequency ω_c.

2.1.1 Four-wave mixing solution

When a small signal with frequency ω_s enters from the left side in Figure 2.1-1 and the time-varying capacitance is modulated by a large pump carrier with a frequency ω_c that propagates in the same direction with the small signal, at each distributed node, the intermodulation tones at $m \cdot \omega_c \pm n \cdot \omega_s, m, n \in Z$ would be generated. One may obtain the solution of Eq. (2.1-2) by only allowing limited tones. When only four tones $\omega_c, \omega_s, \omega_{c-s}, \omega_{c+s}$, are considered as shown in Figure 2.1-2, the following solution Eq. (2.1-5) can de derived which is called a four-wave mixing solution.

$$\begin{cases} V_s(z) = V_0 \cdot \cos(\frac{1}{2\sqrt{2}} \cdot \xi\beta_s z) \\ V_{c-s}(z) = \frac{V_0}{\sqrt{2}} \cdot \frac{\beta_{c-s}}{\beta_s} \sin(\frac{1}{2\sqrt{2}} \cdot \xi\beta_s z) \\ V_{c+s}(z) = \frac{V_0}{\sqrt{2}} \cdot \frac{\beta_{c+s}}{\beta_s} \sin(\frac{1}{2\sqrt{2}} \cdot \xi\beta_s z) \end{cases} \tag{2.1-5}$$

Where the V_0 is the amplitude of the original incident signal and ξ is the capacitance modulation index defined as:

$$\xi = C_1 \cdot V_p / C_0 \tag{2.1-6}$$

Voltage conversion gain can be expressed as in Eq. (2.1-7):

$$G_{c\pm s}(z) = \frac{1}{\sqrt{2}} \cdot \frac{\beta_{c\pm s}}{\beta_s} \sin(\frac{1}{2\sqrt{2}} \cdot \xi\beta_s z) \tag{2.1-7}$$

Voltage gain for the original signal can be expressed as in Eq. (2.1-8):

$$G_s(z) = \cos(\frac{1}{2\sqrt{2}} \cdot \xi\beta_s z) \tag{2.1-8}$$

Eq. (2.1-5) indicates the gradual energy transformation. Signal gradually decays along the propagation, upper and lower converted signals gradually increase along the propagation. For the converted signal, if the capacitance modulation index is large and the transmission line is long, the conversion gain could greater than one. Also, this energy coupling is nonreciprocal. If the time-varying capacitance is modulated by a traveling-wave carrier input from the left side in Figure 2.1-1, energy will convert from the signal and carrier to the frequency-converted signal. However, if the signal and carrier travel in the opposite directions, there is no energy conversion between the signals.

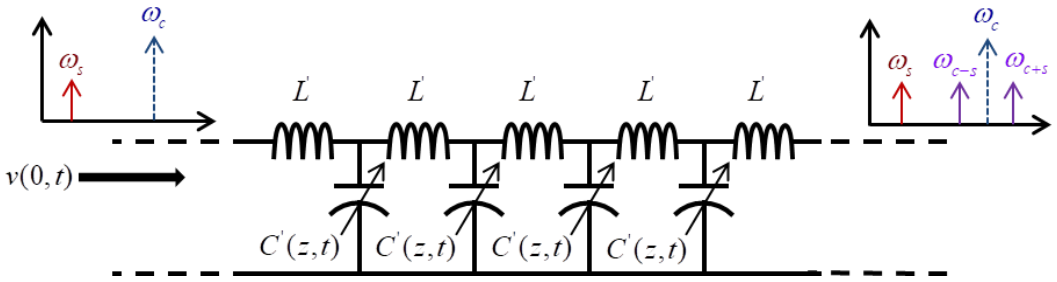

Figure 2.1-2. Lumped-element model of the time-varying transmission line with a four-way mixing condition.

2.1.2 Three-wave mixing solution

If the solution is restricted to three tones [32] to $\omega_c, \omega_s, \omega_{c-s}$ as shown in Figure 2.2-3, Eq. (2.1-9) gives the solution of the three-wave mixing solution:

$$\begin{cases} V_s(z) = V_0 \cdot \cosh(\frac{1}{4}\xi\sqrt{\beta_s\beta_{c-s}}z) \\ V_{c-s}(z) = V_0 \cdot \sqrt{\frac{\beta_{c-s}}{\beta_s}}\sinh(\frac{1}{4}\xi\sqrt{\beta_s\beta_{c-s}}z) \end{cases} \quad (2.1\text{-}9)$$

Voltage conversion gain can be expressed as in Eq. (2.1-10):

$$G_{c-s}(z) = \sqrt{\frac{\beta_{c-s}}{\beta_s}}\sinh(\frac{1}{4}\xi\sqrt{\beta_s\beta_{c-s}}z) \quad (2.1\text{-}10)$$

Voltage gain for the original signal can be expressed as in Eq. (2.1-11):

$$G_s(z) = \cosh(\frac{1}{4}\xi\sqrt{\beta_s\beta_{c-s}}z) \quad (2.1\text{-}11)$$

As seen from Eq. (2.1-10) and Eq. (2.1-11), both original and lower sideband converted signals have the exponential amplification along propagation.

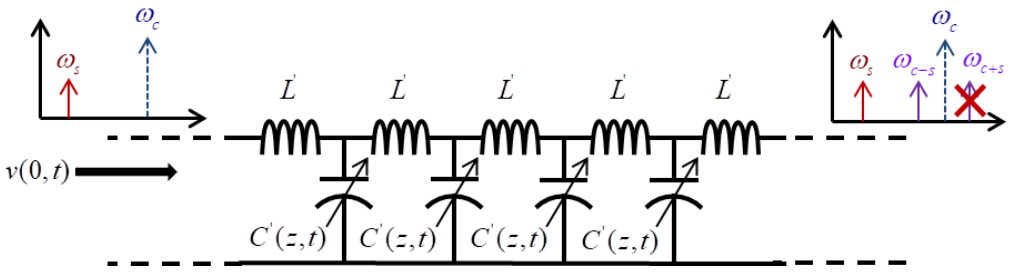

Figure 2.1-3. Lumped-element model of the time-varying transmission line with a three-way mixing condition.

2.1.3 Noise performance of time-varying transmission line

Ideally, the TVTL should not introduce any noise since all components are reactive and lossless. In practice, both the transmission line and time-varying capacitance have a finite quality factor (Q) so that the thermal noise could be generated, which would degrade the noise

performance of the TVTL. The thermal noise generated by the ohmic resistive contributes to the total noise performance, characterized by the noise figure (NF) or noise factor, in two ways. The first one is the TVTL's resistive thermal noise from the original signal ω_s that converted to the converted band $\omega_{c\pm s}$, the second mechanism is the resistive thermal noise from the converted band $\omega_{c\pm s}$ that directly emitted to the output. From [3] Eq. (34), the noise factor of a low loss TVTL can be expressed by Eq. (2.1-12).

$$F = 1 + \frac{1}{3}(1 - e^{-2\alpha_s z}) + \frac{(1-e^{-2\alpha_{c\pm s} z})}{(N g_c)^2} \tag{2.1-12}$$

Where $N g_c$ represents the conversion gain of the TVTL with N units and its value is equivalent to $G_{c\pm s}(z)$ in Eq. (2.1-7) for the four-wave mixing condition or $G_{c-s}(z)$ for the three-wave mixing condition in Eq. (2.1-10). α_s and $\alpha_{c\pm s}$ are the attenuation constants of the transmission line at frequencies ω_s and $\omega_{c\pm s}$. When the loss is small, the following approximation could be applied:

$$\begin{cases} 1 - e^{-2\alpha_s z} \approx 2\alpha_s z = \frac{\beta_s z}{Q_s} \\ 1 - e^{-2\alpha_{c\pm s} z} \approx 2\alpha_{c\pm s} z = \frac{\beta_{c\pm s} z}{Q_{c\pm s}} \end{cases} \tag{2.1-13}$$

Where Q_s and $Q_{c\pm s}$ are the quality factors of the transmission line at the frequencies of ω_s and $\omega_{c\pm s}$ separately. Rewrite Eq. (2.1-12):

$$F = 1 + \frac{1}{3}\frac{\beta_s z}{Q_s} + \frac{1}{G_c^2}\frac{\beta_{c\pm s} z}{Q_{c\pm s}} \tag{2.1-14}$$

Where the G_c is the conversion gain, equals to $G_{c\pm s}(z)$ for the four-wave mixing condition or $G_{c-s}(z)$ for the three-wave mixing condition, of the TVTL.

In Eq. (2.1-14), 1 represents the noise contributed from the source termination, $\frac{1}{3}\frac{\beta_S z}{Q_S}$ represents the noise contribution from the transmission line's thermal noise from the original signal band and $\frac{1}{G_c^2}\frac{\beta_{c\pm s} z}{Q_{c\pm s}}$ represents the noise contribution from the transmission line's thermal noise at the converted band. Given by Eq. (2.1-14), the noise factor of the TVTL could achieve only one-third of the original transmission line's noise factor when the conversion gain of the TVTL is large and the transmission line is long.

2.2 Circuit Realization of Time-varying Transmission Line

In the real circuit implementation of the TVTL, time-varying capacitance is realized by reversed biased varactor diodes and the TVTL is realized by transmission line with periodically loaded varactor diodes. For the purpose of decreasing the area, improving power efficiency and conversion gain, inductor-pumped TVTL, and M-derived TVTL are developed. A detailed discussion is followed.

2.2.1 Prior work

The most prior work [7] is shown in Figure 2.2-1, which is a PCB version TVTL. Figure 2.2-1(a) and Figure 2.2-1(b) show the 3-D implementation and planar implementation of the PCB version TVTL. The schematic is very straightforward which is the transmission line with periodically loaded varactor diodes. Good matching could be achieved by properly designing the Bloch impedance of the periodic structure. After the passband of the periodic structure is determined, the capacitance of the varactor diodes, length and characteristic impedance of the transmission line can also be calculated. The biasing point of the varactor is chosen to be having the varactor diode's the best modulation index ξ. This TVTL uses fully differential structure, the carrier, and the signal are both in the differential fashion and propagate in totally separate paths, so good isolation between carrier and signal is achieved. The practical implementation of the PCB version TVTL is shown in Figure 2.2-1 (c).

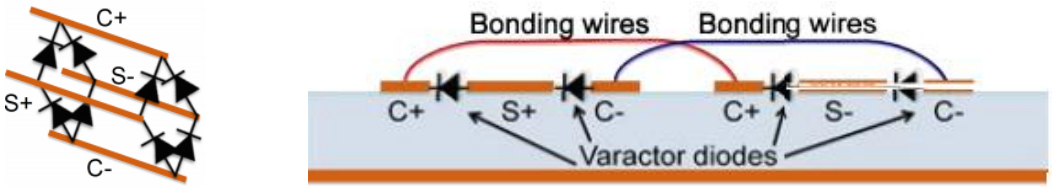

(a) (b)

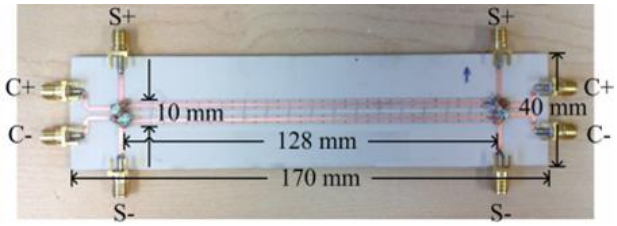

(c)

Figure 2.2-1. (a)3-D implementation of the PCB version TVTL, (b)Planar implementation of the PCB version TVTL, (c)Fabricated PCB version TVTL.

In order to minimize the size, MMIC version TVTL is also designed and fabricated, schematic and layout are shown in Figure 2.2-2(a) and Figure 2.2-2(b). Because of a lack of flexibility on the MMIC design, carrier and signal need to be combined through an external combiner and fed into the TVTL. Meander line is used to minimize the size of the chip.

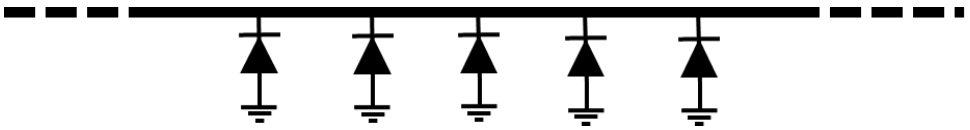

(a)

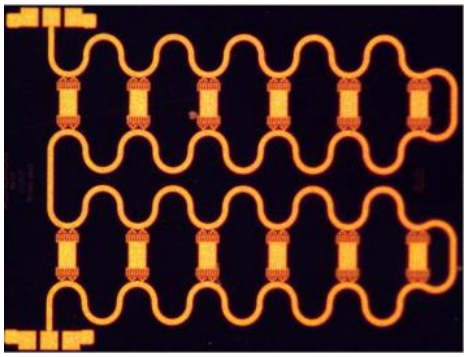

(b)

Figure 2.2-2. (a)Schematic of MMIC version TVTL, (b)Layout of MMIC version TVTL ($0.2\mu m$ GaN HEMT technology, size of the chip is $1.5mm \cdot 2.5mm$).

2.2.2 Inductor-pumped and M-derived TVTL

From Eq. (2.1-7) and Eq. (2.1-10), the conversion gain is strongly related to the modulation index ξ of the capacitance. A large modulation index ξ could be realized by a large carrier power which is not power efficient, a better way is to use inductor-pumped structure as shown in Figure 2.2-3 to boost ξ. A small inductor is placed in series with the varactor diode to create a resonance. Eq. (2.2-1) and Eq. (2.2-2) show how it works.

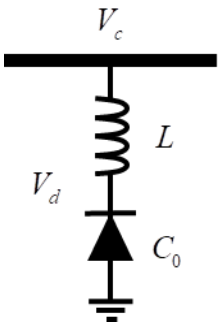

Figure 2.2-3. A single unit of the inductor-pumped structure.

In Eq. (2.2-1), V_c is the applied carrier voltage amplitude and V_d is the voltage amplitude across the varactor diode. By creating a series LC resonance between the inductor L and the varactor, as $\omega_c^2 LC_0$ approaching to 1, the modulation voltage V_d across the varactor could be significantly increased and resulting in an effective capacitance modulation ξ' as shown in Eq. (2.2-2).

$$\frac{V_d}{V_c} = \frac{1/(j\omega_c C_0)}{j\omega_c L + 1/(j\omega_c C_0)} = \frac{1}{1-\omega_c^2 LC_0} \tag{2.2-1}$$

$$\xi' = \frac{1}{1-\omega_c^2 LC_0}\xi \tag{2.2-2}$$

Even though the capacitance modulation index could be increased by adding an inductor, the structure of the inductor-pumped TVTL suffers two drawbacks. First, by adding the series inductor, the bandwidth of the TVTL will be changed and shrank because of the resonance. Second, the transmission line could still occupy a large chip area. The M-derived TVTL overcomes these problems. Figure 2.2-4 shows the schematic of the M-derived TVTL which replaces the transmission line with the inductors. The design procedure follows the filter design method as image parameter method [32], by designing the M-derived filter section, the cutoff frequency, capacitance value, and inductor values could be determined.

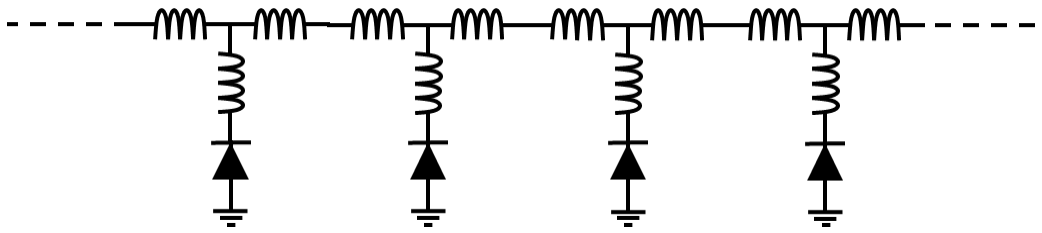

Figure 2.2-4. Schematic of the M-derived TVTL.

The M-derived TVTL is designed on MMIC and fabricated with Global Communication Semiconductors (GCS) InGaP HBT process. The fabricated TVTL chip is shown in Figure 2.2-5, which is composed of 10 periodic M-derived units series connected in the middle and two matching units at both sides. Varactor diode's I-V curve is shown in Figure 2.2-6, the average capacitance of the varactor diodes is designed to be around $0.45pF$ with the size of $3 \cdot 10\mu m \cdot 50\mu m$. The series and shunt inductors are designed to be $1.2nH$ and $0.3nH$ separately. The overall chip size is $4020\mu m \cdot 1520\mu m$.

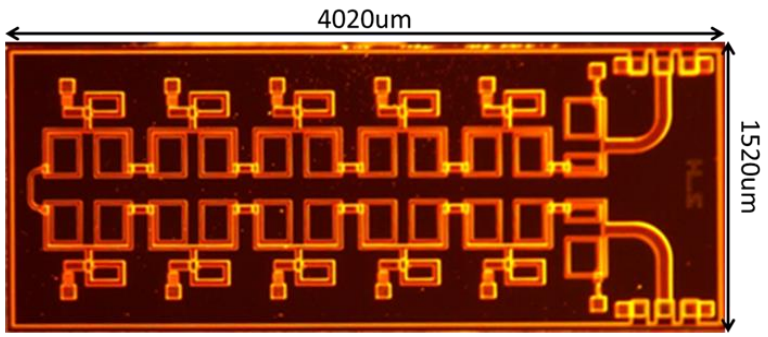

Figure 2.2-5. Layout of the fabricated 10-unit M-derived TVTL.

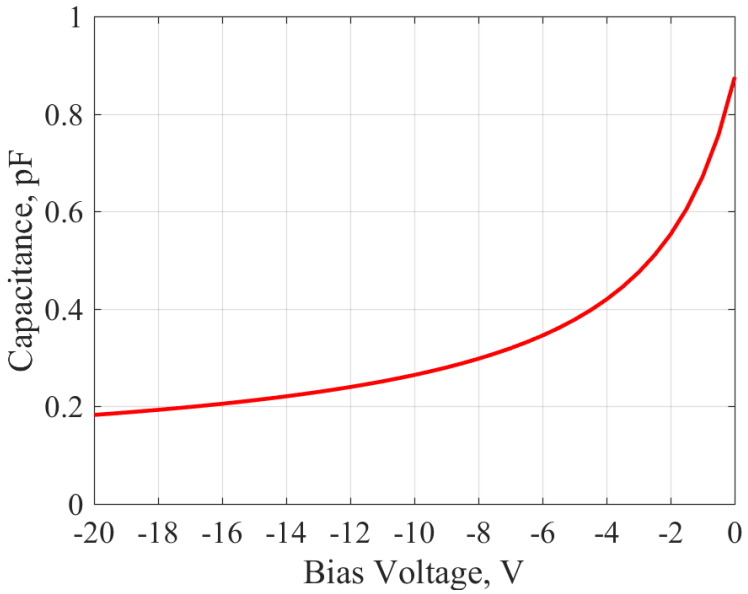

Figure 2.2-6. The I-V curve of the varactor diode with the size of $3 \cdot 10\mu m \cdot 50\mu m$.

The cutoff frequency of this TVTL is designed to be up to $5.5GHz$. Figure 2.2-7 shows the simulated and measured S-parameter with the biasing voltage at $-2.8V$ and $-4V$.

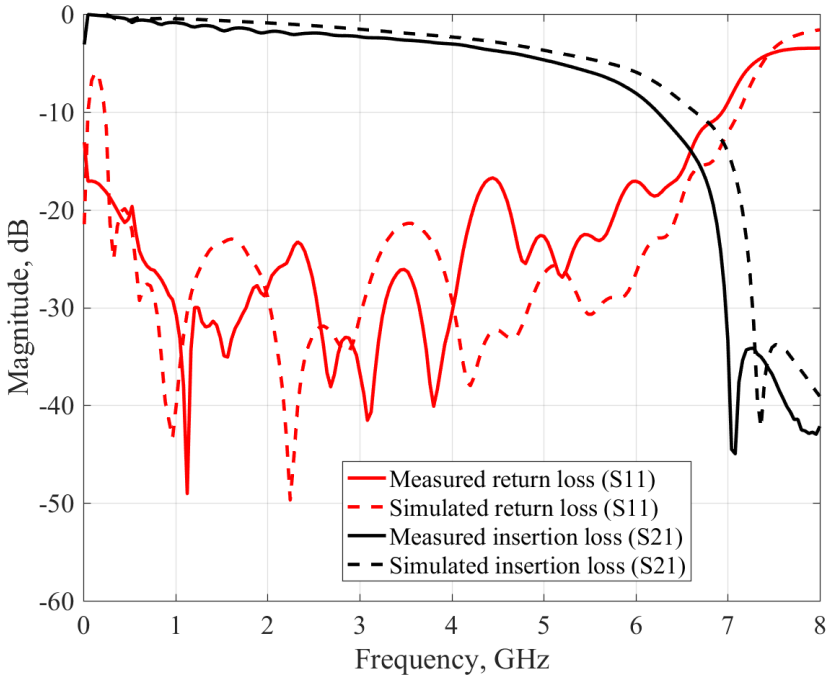
Magnitude, dB
Frequency, GHz
Measured return loss (S11)
Simulated return loss (S11)
Measured insertion loss (S21)
Simulated insertion loss (S21)

(a)

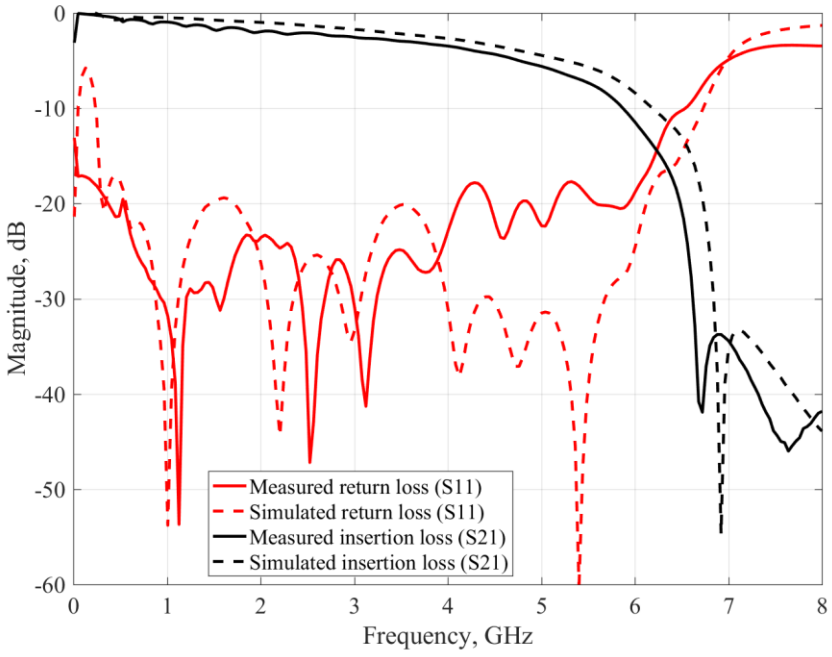
Magnitude, dB
Frequency, GHz
Measured return loss (S11)
Simulated return loss (S11)
Measured insertion loss (S21)
Simulated insertion loss (S21)

(b)

Figure 2.2-7. (a)Simulated and Measured S-parameter of the TVTL with varactor biased at $-2.8V$, (b)Simulated and Measured S-parameter of the TVTL with varactor biased at $-4V$.

The conversion gain is measured by Performance Network Analyzer (PNA-X) that has the build-in mixer and noise figure measurement function. Both carrier and signal are combined through an external diplexer and fed into the TVTL. At the output of the TVTL, another diplexer is used to separate carrier and the converted signal, conversion gain is examed by PNA-X. A bias tee is added to bias the TVTL to be at$-2.8V$, the input signal is measured from $0.6GHz - 1.2GHz$ with power of $-10dBm$ and pump carrier is at $4.3GHz$ with power $27dBm$. The solid black line in Figure 2.2-8 shows the conversion gain of the TVTL after the de-embedded losses of the input and output diplexers, the blue dash line is the simulated conversion gain by using Advanced Design System (ADS) Harmonic Balance (HB) simulation, the red dash line is the theoretical conversion gain predicted by Eq. (2.1-7), a four-wave mixing conversion condition, with an additional loss factor $e^{-\alpha z}$ included, where the α is an attenuation constant that averages both the original signal and converted signal propagation loss. The results show an overall less than $2.5dB$ conversion loss for the entire band and a positive conversion gain from $0.6GHz - 0.75GHz$.

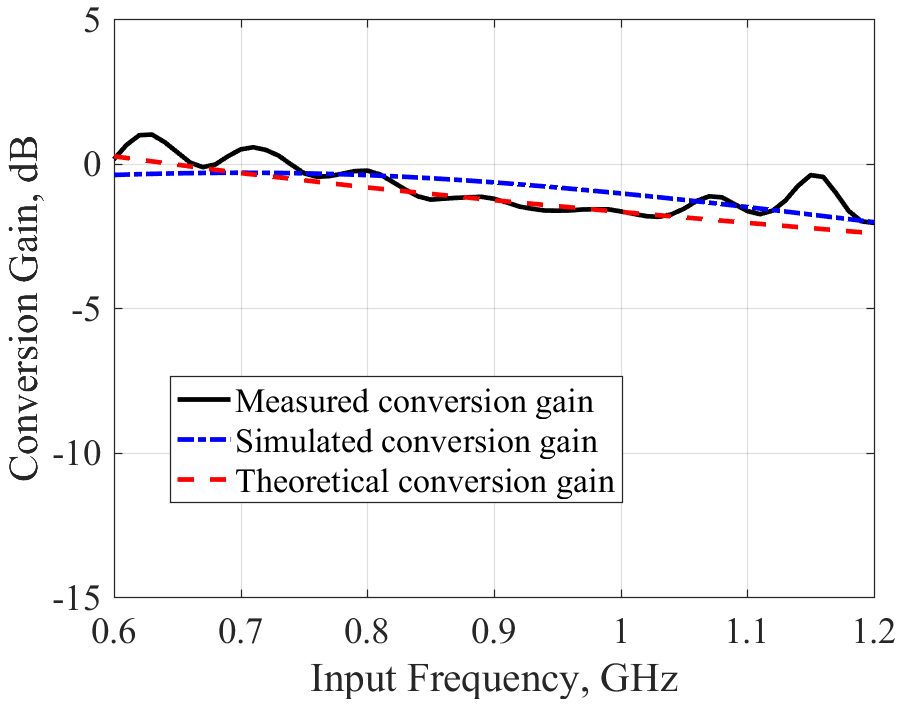

Figure 2.2-8. Measured, simulated, and theoretical conversion gain of the designed M-derived MMIC TVTL under the varactor biased at $-2.8V$ and carrier frequency at $4.3GHz$ with power of $27dBm$.

Low-noise and high-sensitive receiver in PNA-X enables its noise figure measurement ability. The test setup is very similar to the conversion gain measurement besides two bandpass filters are added. The first bandpass filter is connected after the carrier source and before the diplexer to filter out the noise from the carrier source at the converted band ω_{c-s}, the second bandpass filter is connected at the TVTL's output diplexer for protecting the PNA-X's receiver. Because of the availability of the filters, the input signal is from $0.76GHz - 0.79GHz$ with the power of $-10dBm$ and carrier power is set to $27dBm$ at $4.3GHz$. Figure 2.2-9 shows the measured, simulated, and theoretical predicted noise figures. Simulation is finished by ADS HB

and the theoretical result is calculated according to Eq. (2.1-14). An average measured noise figure of $2.8dB$ is observed in the entire frequency range.

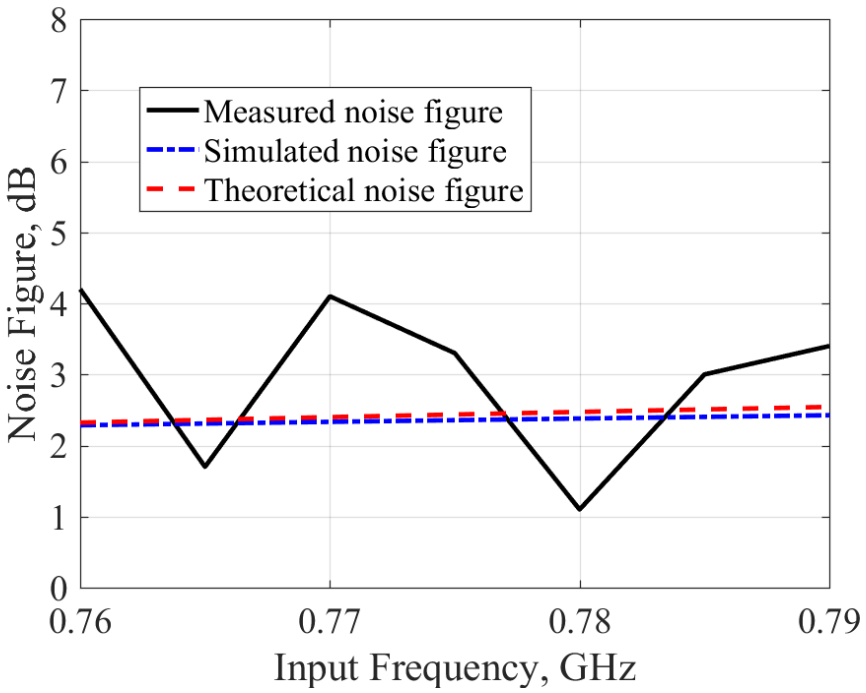

Figure 2.2-9. Measured, simulated, and theoretical noise Figure of the designed MMIC TVTL under the varactor biased at $-2.8V$ and carrier frequency at $4.3GHz$ with power of $27dBm$.

Another set of the conversion gain is measured under the condition of the carrier frequency of $5.4GHz$ with the power of $25dBm$ and signal is from $0.8GHz - 1.2GHz$ with $-10dBm$ power. Based on S-parameter measurement results from Figure 2.2-7(b), the upper sideband of the converted signal $6.2GHz - 6.6GHz$ falls into the stopband of the TVTL, which enables the TVTL works at the three-wave mixing condition as indicated in Eq. (2.1-10). Figure 2.2-10 shows the measured conversion gain, the simulated result which is simulated by ADS HB and theoretical conversion gain predicted by Eq. (2.1-10) with an extra loss correction term, an

additional loss factor $e^{-\alpha z}$ that based on S-parameter result. The conversion gain is around $-2dB$, compared with the conversion gain for the four-wave mixing condition at the same frequency band, three-way mixing has a better power efficiency.

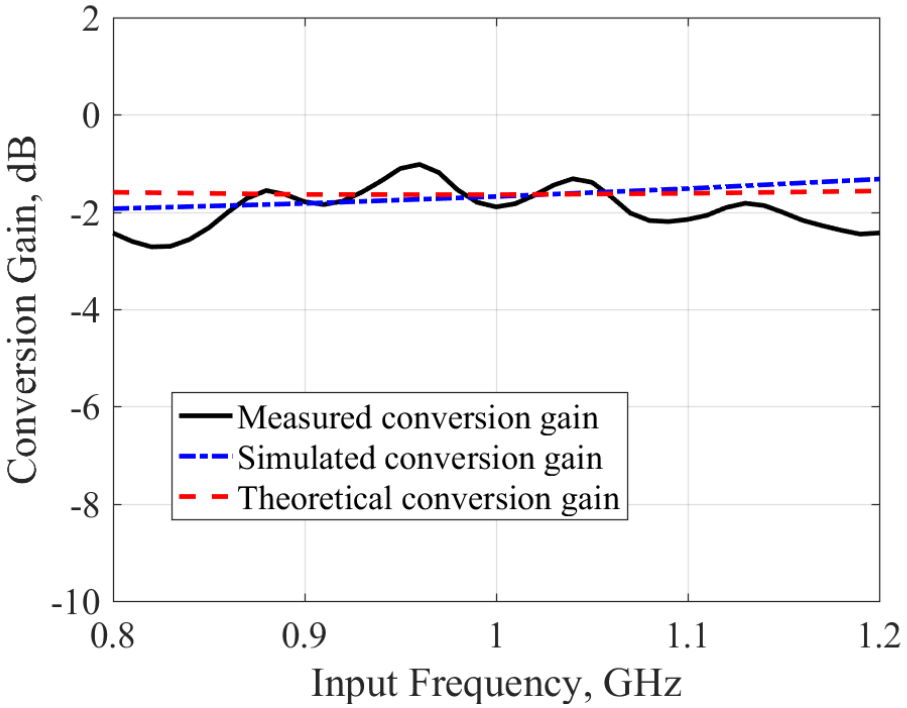

Figure 2.2-10. Measured, simulated, and theoretical conversion gain of the designed MMIC TVTL under the varactor biased at $-4V$ and carrier power of $25dBm$.

Chapter 3

Correlator Operating Principle, Correlation Experimental Setup and Results

In-band jamming/interference could be alleviated by performing direct correlation at the RF front-end through coding and decoding. Usually, any operation at the RF front-end requires low loss, low noise, and high power handling capability. The time-varying transmission line (TVTL) based on correlator is proposed for this purpose.

3.1 Correlation at RF Domain

The basic correlation operation is depicted in Figure 3.1-1. The received signal is multiplied with a reference signal, and the product of these two signals is fed into an integrator which integrates over a specific time interval.

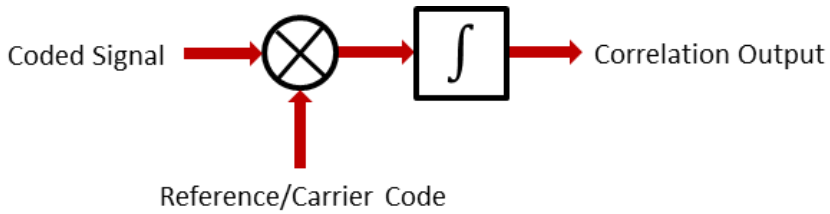

Figure 3.1-1. Correlation operation.

A detailed RF signal processing diagram is shown in Figure 3.1-2 which illustrates how the correlator, an RF signal processing block, is capable of rejecting the jammer and noise. The received signals at the antenna side are composed of three parts: desired signal, noise jammer

and tone jammer. Multiplication is performed at the first stage in the correlator with a reference code. Since the desired signal is correlated/coherent with the reference code that the wideband desired signal is to be dispreaded into a narrow band signal. However, when noise jammer and tone jammer are multiplied with the reference, these signals are spread out. After the multiplication, all these signals are filtered by a high-Q bandpass filter that passes the desired narrowband signal. Time domain and frequency domain signals are all depicted in Figure 3.1-2. Signal-to-noise ratio (SNR) is increased proportionally to the reduction of instantaneous bandwidth of the desired signal.

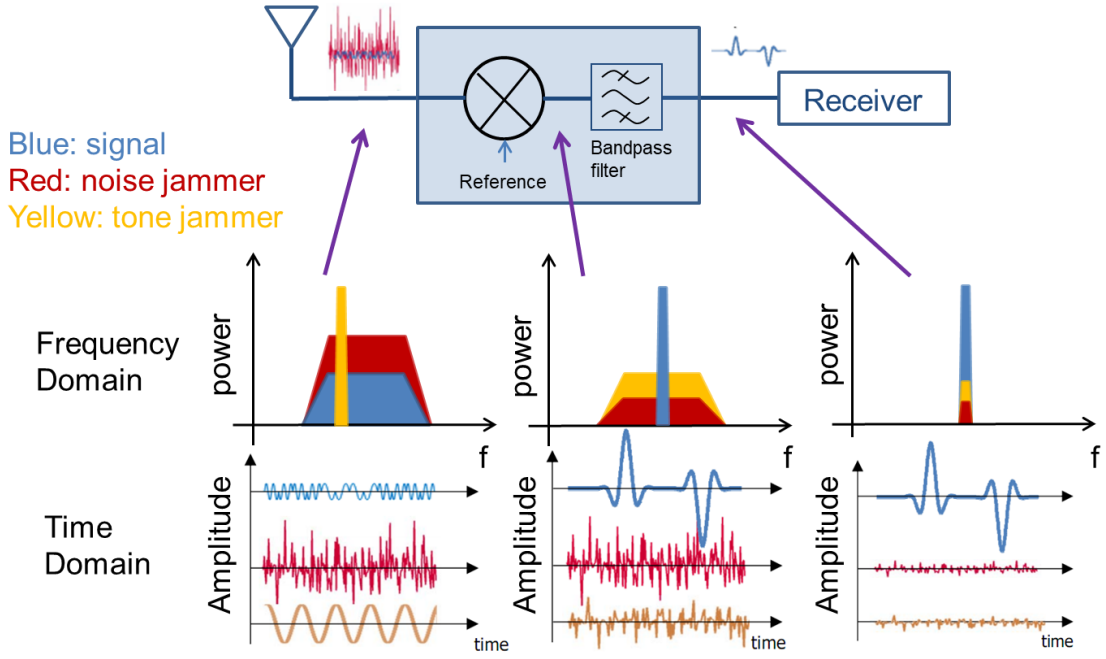

Figure 3.1-2. Signal processing at the RF domain.

RF correlators can operate as spread spectrum encoder/decoder for the benefits in rejecting interferences. For the full system's benefit, they must be placed in the very front of the RF system, before Low Noise Amplifier (LNA) and after Power Amplifier (PA).

3.2 Open Loop Correlator and Experimental Setup and Results

An open loop correlator is designed and tested in this session.

3.2.1 Open loop time-varying transmission line correlator

The Schematic of the open loop TVTL correlator is shown in Figure 3.2-1. Signal and reference/carrier are combined, fed into the TVTL through a diplexer. The mixing is carried out through parametric modulation at each varactor diode and the upconverted signal is combined distributedly to form a positive gain. Integration is performed by a fixed frequency high-Q bandpass filter added at the output of the TVTL, which also offers a bandwidth selection property. The practical implementation of the open loop TVTL correlator is shown in Figure 3.2-2.

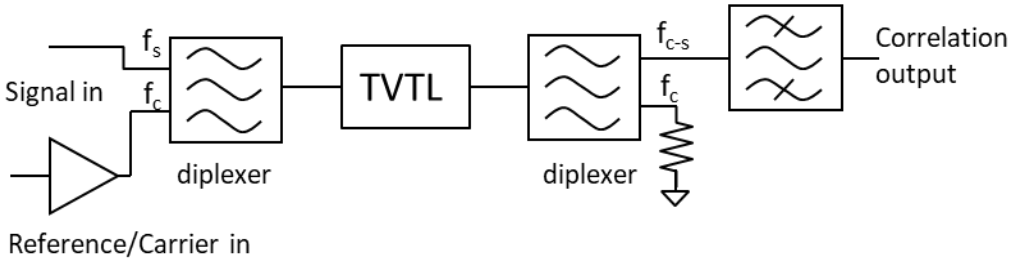

Figure 3.2-1. Schematic of the open loop correlator.

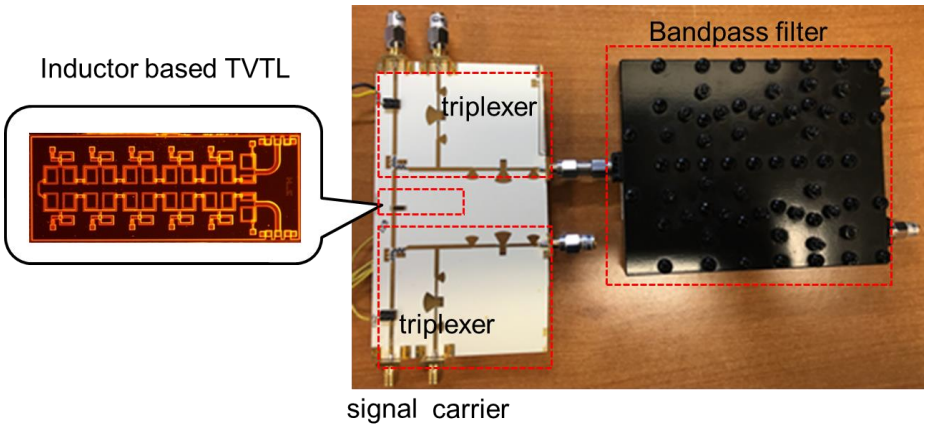

Figure 3.2-2. Implementation of the open loop correlator.

3.2.2 Open loop time-varying transmission line correlator test setup and results

Comprehensive tests for the open loop TVTL correlator are performed in this session, which includes frequency response, noise figure, $P1dB$, linearity, and correlation tests.

The bandpass filter used in this design has a center frequency of $f_{BPF} = 3.525GHz$ with $3dB$ bandwidth of $50MHz$. The dash lines show the frequency-shifted versions of its S_{21} in Figure 3.2-3. when the TVTL is placed in front of the filter while altering the reference/carrier frequency f_c, it corresponds to select the correlation band of $f_c - f_{BPF}$. The reference/carrier is changed from $4.2GHz - 4.7GHz$ and the frequency response of the correlator is shown in Figure 3.2-3 drawn with solid lines. The minimum insertion loss of the open loop correlator including the output bandpass filter is $2.8dB$ at the reference/carrier of $4.4GHz$. The measured noise figure under the condition of reference/carrier at $4.3GHz$ is shown in Figure 3.2-4. The noise figure is around $5.5dB$ which slightly larger than the conversion loss ($4.2dB@4.3GHz$) of the entire open loop correlator. The measured noise figure indicates that the TVTL chip does not introduce a significant amount of noise which makes the property of the entire open loop correlator's noise

figure similar to a passive device. The input $P1dB$ of the designed circuit is measured at $4.4GHz$, as shown in Figure 3.2-5, which reaches to a maximum value of $18dBm$.

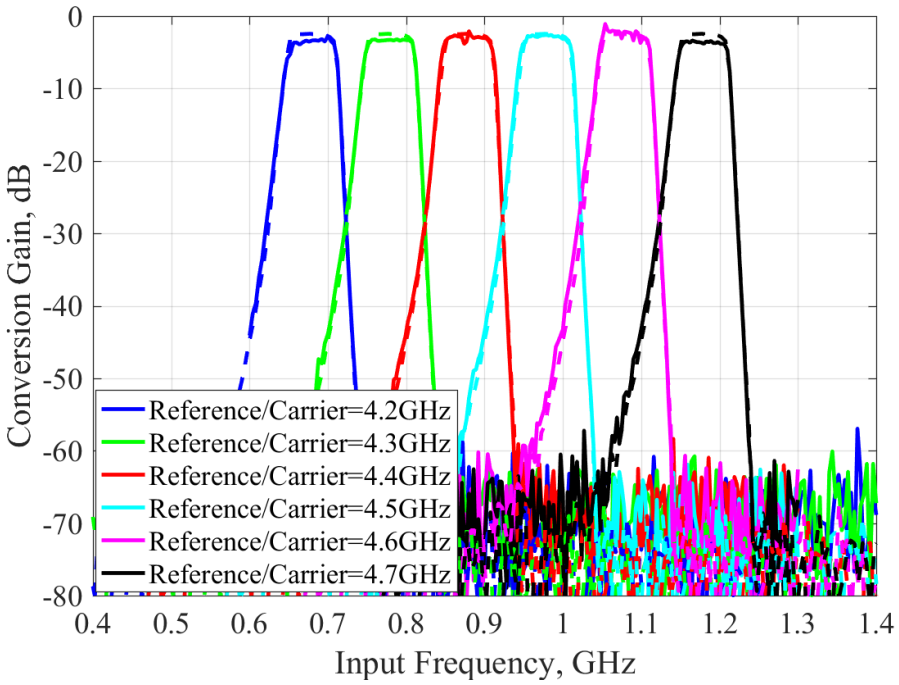

Figure 3.2-3. Measured conversion gain of the open loop correlator after the bandpass filter with varactor biased at $-2.8V$, reference/carrier power of $28dBm$ at $4.2GHz - 4.7GHz$.

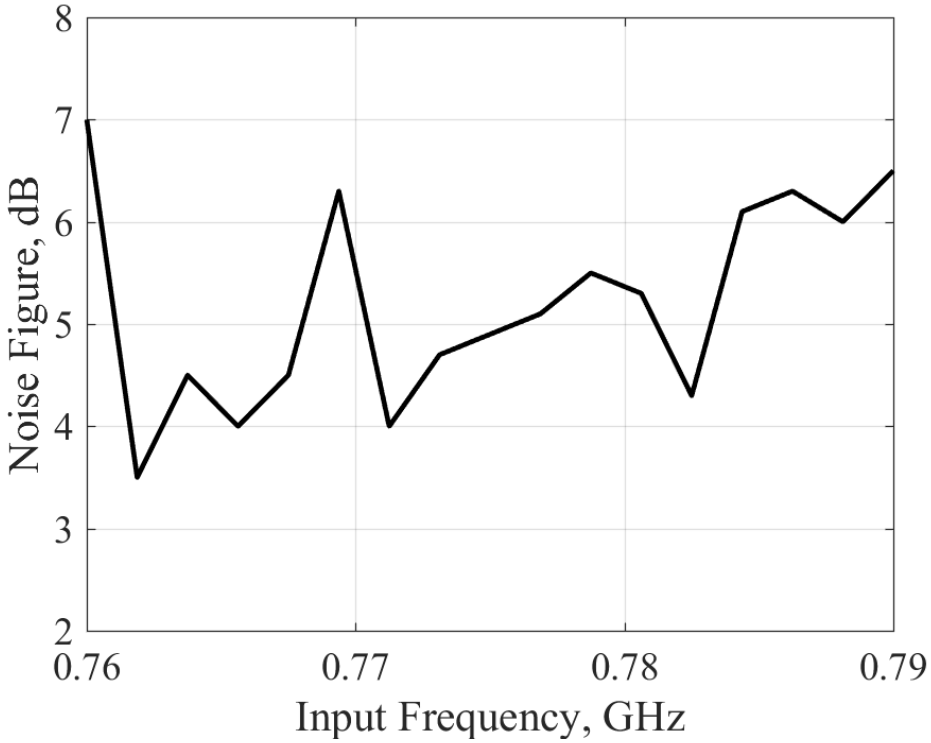

Figure 3.2-4. Measured noise figure of the open loop correlator with varactor biased at $-2.8V$, reference/carrier power of $28dBm$ at $4.3GHz$.

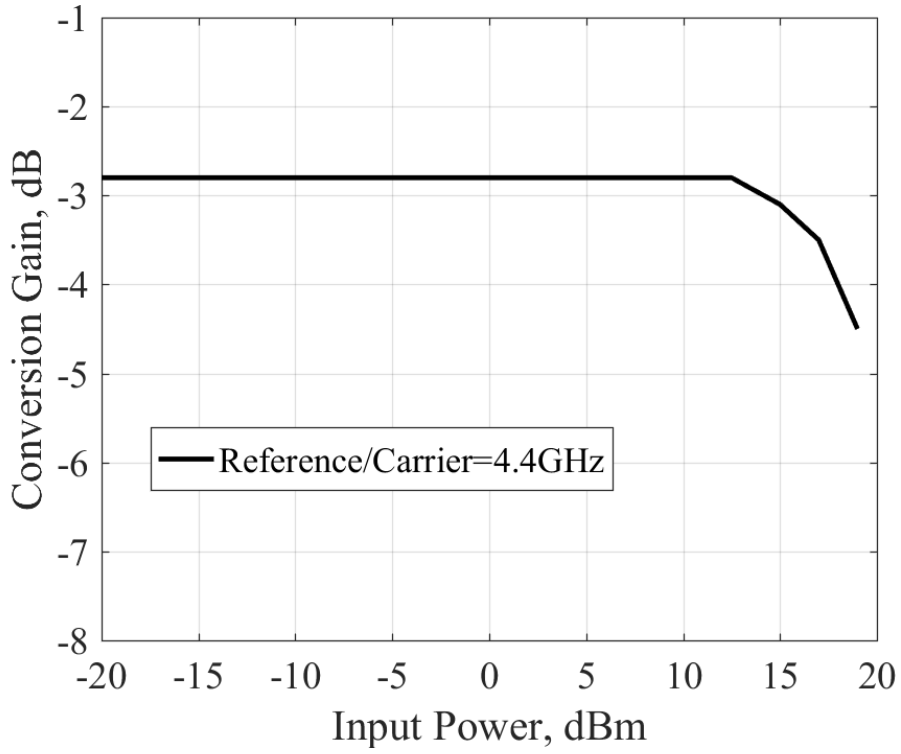

Figure 3.2-5. Measured conversion gain of the open loop correlator versus input power with varactor biased at $-2.8V$, reference/carrier power of $28dBm$ at $4.4GHz$.

The two-tone $IM3$ test is carried out to derive the $IIP3$ by using Eq. (3.2-1), where the $IM3$ is the power difference between the main tone with the sidetone and P_{in} is the power of the input signal. Two-tone input frequencies are located at $870MHz\&880MHz$ with $10MHz$ apart and carrier pump power is set to $28dBm$. The measured spectrum is shown in Figure 3.2-6 and the measured $IIP3$ is equal to $20.7dBm$.

$$IIP3 = \frac{IM3}{2} + P_{in} \tag{3.2-1}$$

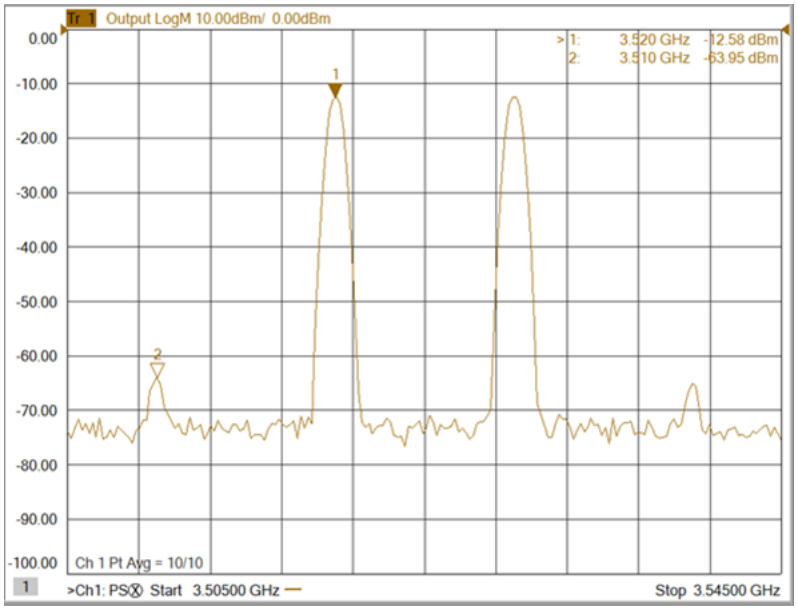

Figure 3.2-6. Measured spectrum of the two-tone *IM*3 test of the open loop correlator.

Correlation test and decoder test are carried out by modulating both the signal and reference/carrier with correlated and orthogonal codes. Diagram of the test setup is shown in Figure 3.2-7, Arbitrary waveform generator (AWG) generates two modulated signals, one is for the received signal, another one is mixed to the reference/carrier band and amplified to the right level. Both signal and reference/carrier are fed into the open loop TVTL correlator and the output signal is observed by either oscilloscope or spectrum analyzer.

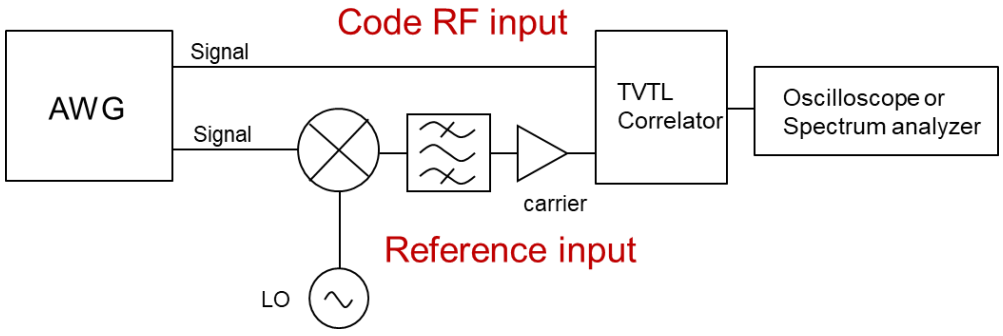

Figure 3.2-7. Correlation test and decoder test setup.

Binary Amplitude Shifting Keying (BASK), Binary Phase Shifting Keying (BPSK) and Frequency Shifting Keying (BFSK) are used to exam the frequency domain correlation. For all these three modulation schemes, the bit rate is set to $200M/s$, integration bandwidth is equal to $50MHz$ which is the same as the bandwidth of the high-Q bandpass filter, and no pulse shaping is applied.

The first frequency domain correlation test is carried out by modulating both the signal and reference/carrier with correlated and orthogonal BASK code. The center frequencies of signal and reference/carrier are at $0.8GHz$ and $4.4GHz$ separately. Repeated binary codes are mapped to BASK as shown in Figure 3.2-8, the correlated codes for both signal and reference/carrier used in the measurement are with the identical code, while the orthogonal codes are with the flipped amplitude. Figure 3.2-9 shows the correlation spectrum at the output of the correlator. A sharp peak is observed in Figure 3.2-9(a) when signal and reference/carrier are modulated with coherent codes and synchronized in time. A minor spectrum regrowth is observed which is caused by symbol misalignment. A notch is observed in Figure 3.2-9(b) when signal and reference are modulated with orthogonal codes. Approximated $15dB$ correlation suppression is thus obtained by comparing these two cases.

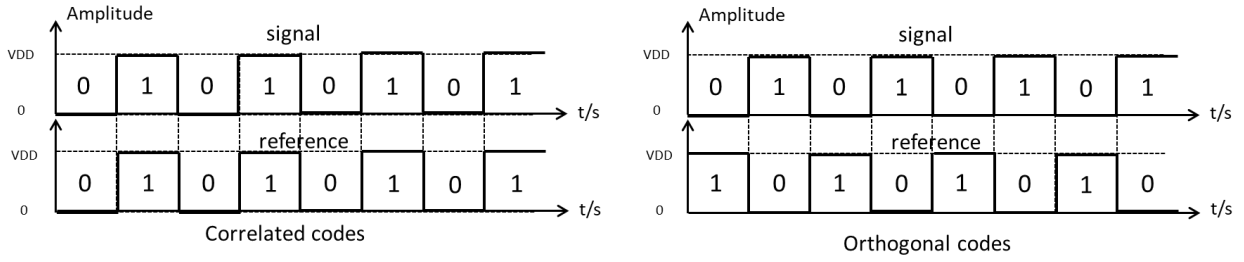

Figure 3.2-8. Orthogonal and correlated BASK codes used in the correlation test.

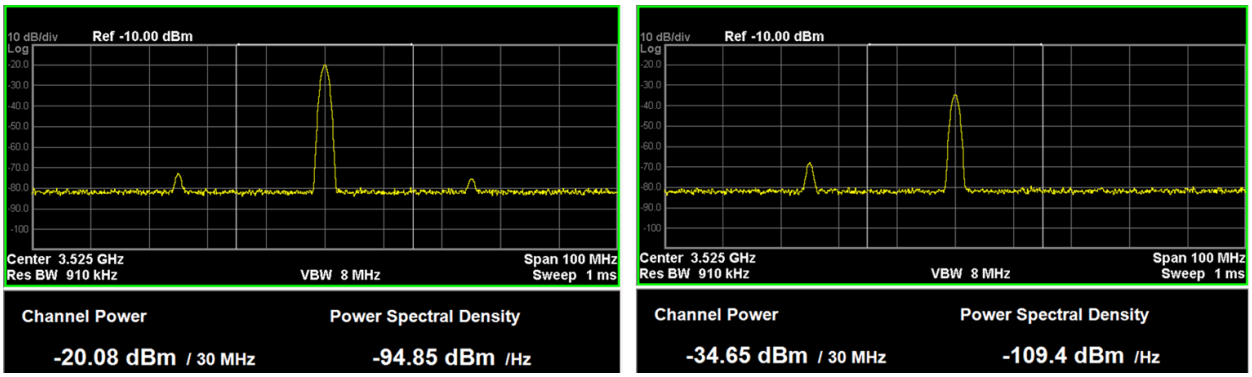

(a) (b)

Figure 3.2-9. (a)Correlation spectrum of the signal and the reference/carrier modulated with correlated BASK codes, (b)Correlation spectrum of the signal and the reference/carrier modulated with orthogonal BASK codes.

Another frequency domain correlation test is carried out by using BPSK code. The center frequencies of the signal and reference/carrier are at $0.8GHz$ and $4.4GHz$ separately. For the correlated codes, the signal and reference/carrier are with the same phase shift, but there is no phase shift for the orthogonal codes as shown in Figure 3.2-10. Figure 3.2-11 shows the correlation spectrum of the two cases, by comparison, $44dB$ correlation suppression is achieved.

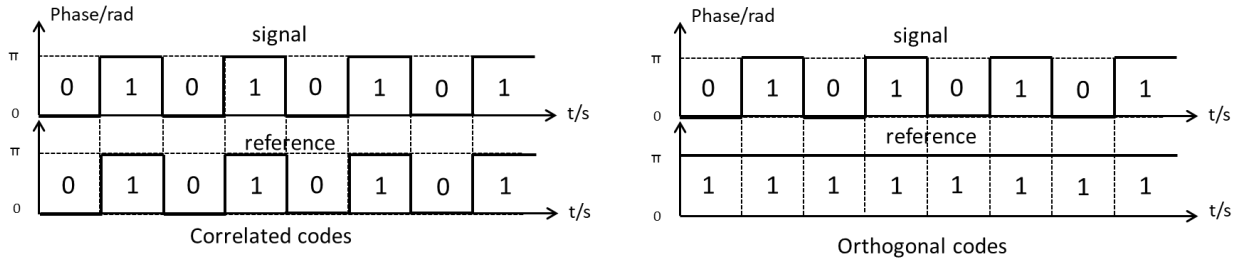

Figure 3.2-10. Orthogonal and correlated BPSK codes used in the correlation test.

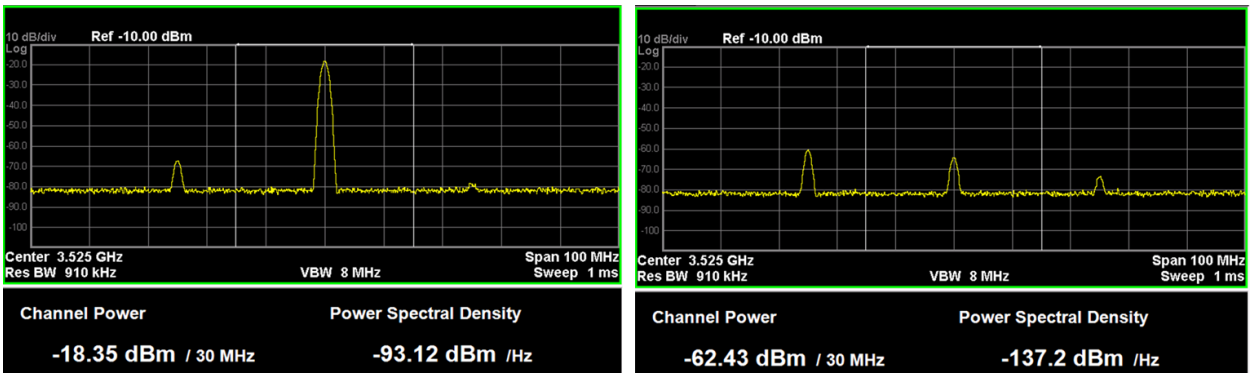

(a) (b)

Figure 3.2-11. (a)Correlation spectrum of the signal and the reference/carrier modulated with correlated BPSK codes, (b)Correlation spectrum of the signal and the reference/carrier modulated with orthogonal BPSK codes.

Figure 3.2-12 shows the orthogonal and correlated BFSK codes used in the frequency domain correlation test. The center frequencies of signal and reference/carrier are at $0.8GHz$ and $4.4GHz$ separately, the frequency shift is set to $0.275GHz$. Correlated codes are with identical frequency shift, orthogonal codes are in complementary frequency shift. Close to $20dB$ correlation suppression is reached as shown in Figure 3.2-13.

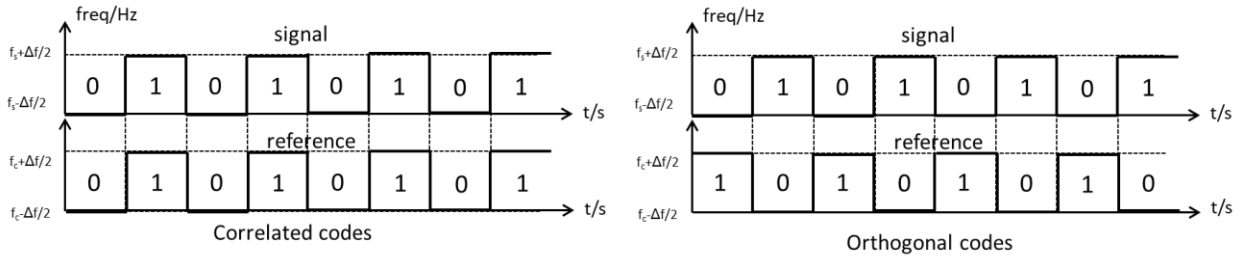

Figure 3.2-12. Orthogonal and correlated BFSK codes used in the correlation test.

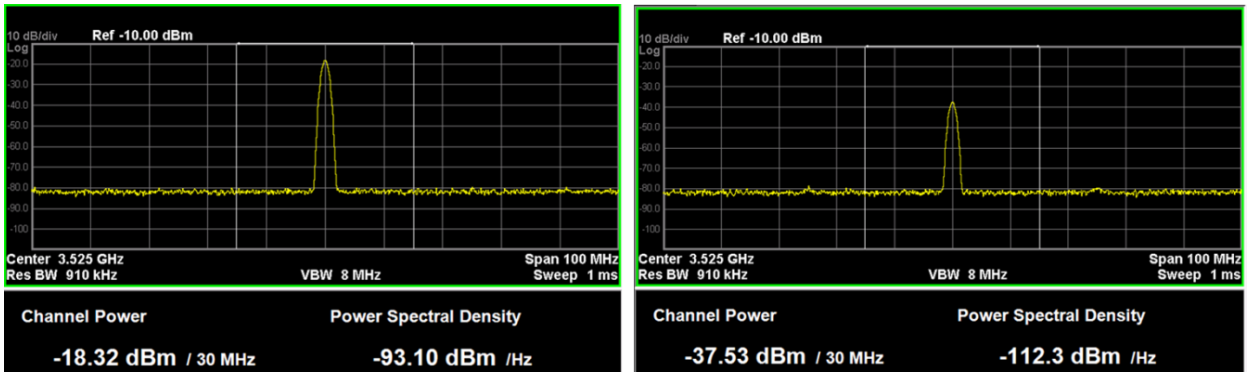

(a) (b)

Figure 3.2-13. (a)Correlation spectrum of the signal and the reference/carrier modulated with correlated BFSK codes, (b)Correlation spectrum of the signal and the reference/carrier modulated with orthogonal BFSK codes.

The time-domain decoder is tested under the direct-sequence spread spectrum (DSSS) scheme. Like frequency domain correlation tests, three different modulations, BASK, BPSK, and BFSK are used and one symbol is composed of four chips with a chip rate of $200M/s$. The codes of the reference/carrier and signal for BASK modulation are depicted in Figure 3.2-14, symbol 1 and symbol 0 are mapped into spread chips, and these two symbols are sent repeatedly. Figure 3.2-15 shows the voltage waveform at the output of the designed correlator and the envelope of the waveform with peak to valley ratio of $4{:}\,1$ with a symbol rate of $50M/s$ directly shows the demodulated symbol.

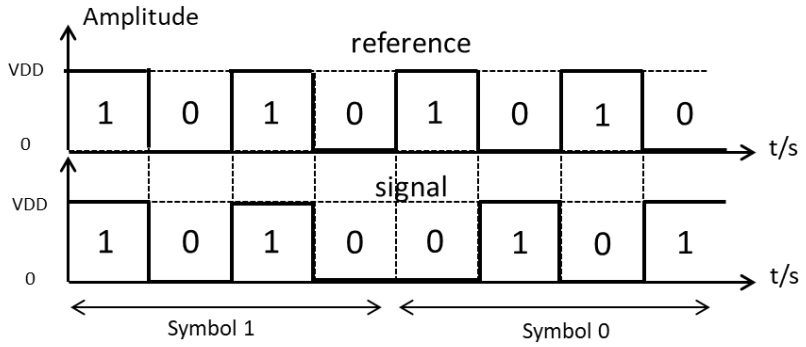

Figure 3.2-14. Reference/carrier and signal BASK codes used in the time domain decoder test.

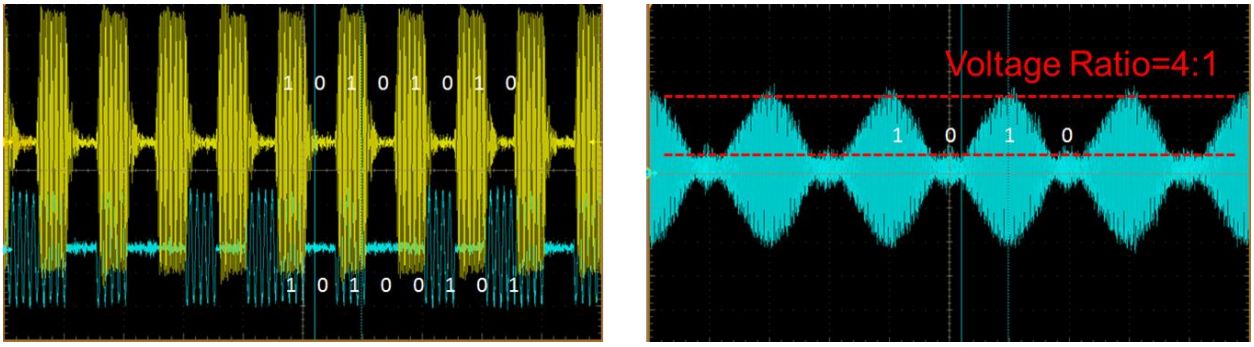

(a) (b)

Figure 3.2-15. (a)Signal (blue) and reference (yellow) waveforms for time-domain decoder test, (b)Waveform at the output of the correlator.

In the decoder test by using the BPSK codes, symbol 1 is represented by 4 chips of $-1,1,-1,1$, and reference/carrier code is the same, symbol 0 is the continuous wave without phase flip as shown in Figure 3.2-16. The envelope at the correlator output waveform shows the demodulated symbol.

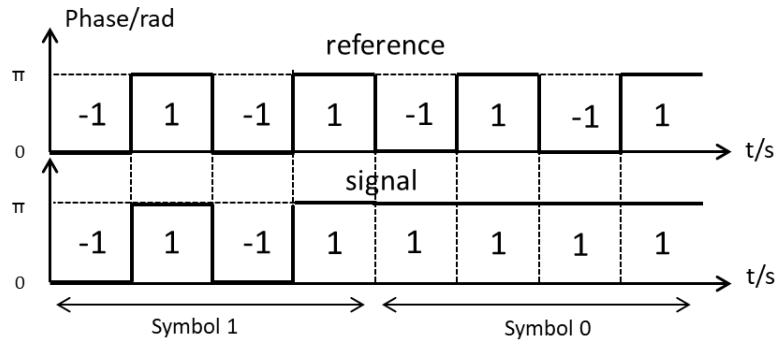

Figure 3.2-16. Reference/carrier and signal BPSK codes used in the time domain decoder test.

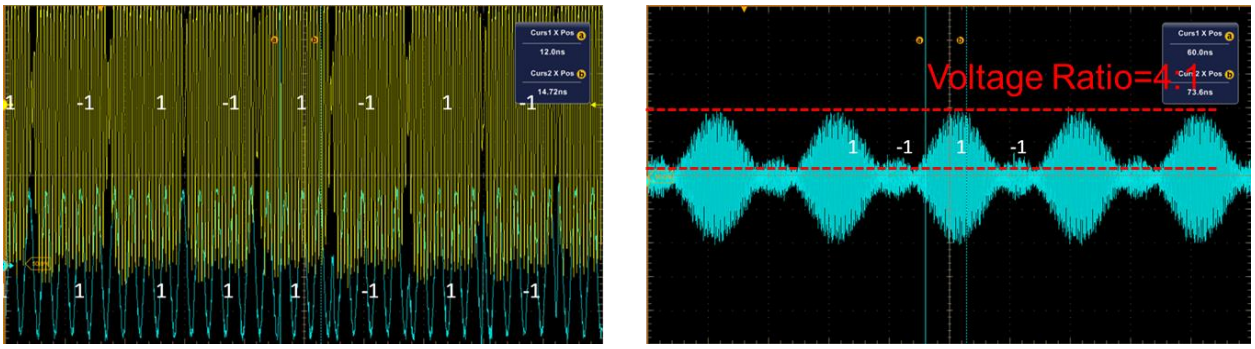

(a) (b)

Figure 3.2-17. (a)Signal (blue) and reference (yellow) waveforms for time-domain decoder test, (b)Waveform at the output of the correlator.

Figure 3.2-18 shows the spread sequence symbols of BFSK codes and Figure 3.2-19 shows the demodulated symbols at the output of the correlator.

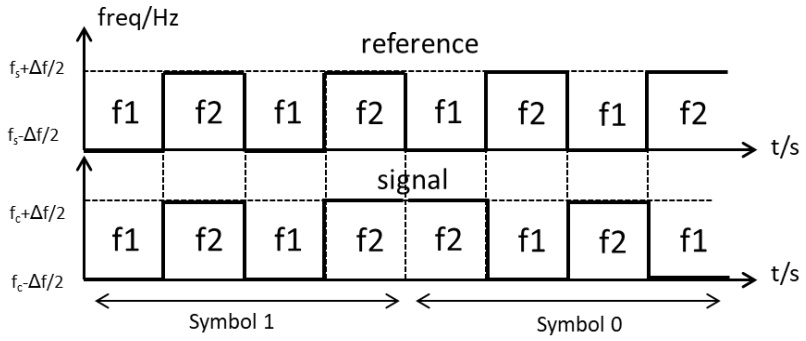

Figure 3.2-18. Reference/carrier and signal BFSK codes used in the time domain decoder test.

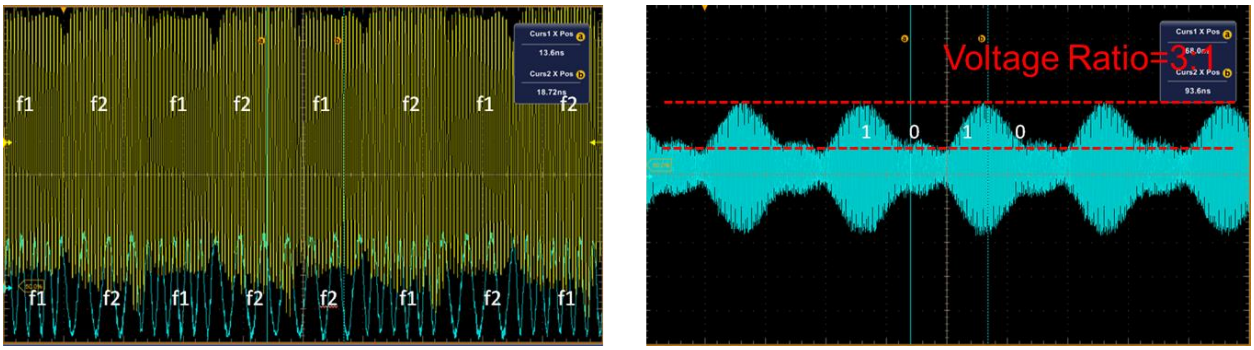

(a) (b)

Figure 3.2-19. (a)Signal (blue) and reference (yellow) waveforms for time-domain decoder test, (b)Waveform at the output of the correlator.

3.3 Closed Loop Correlator and Experimental Setup and Results

A different setup of the correlator can be formed by closed loop TVTL. Similar to the open loop TVTL correlator, the multiplication is fulfilled by the capacitive mixing at the varactors. However, integration is now realized by creating a feedback path for the upconverted signal.

3.3.1 Ring resonance at lower sideband

The TVTL can be treated as a frequency mixer that exchanges frequency components [33] from ω_s to ω_{c-s} and vice versa. Assuming that the incident waves are at the frequencies of ω_s, ω_{c-s} and in the same direction with carrier wave that is pumped at the frequency at ω_c. A symbol of TVTL cross-coupling between ω_s and ω_{c-s} under the carrier of ω_c is shown in Figure 3.3-1(a). The equation Eq. (3.3-1) shows the matrix of the coupling across different frequencies at different ports.

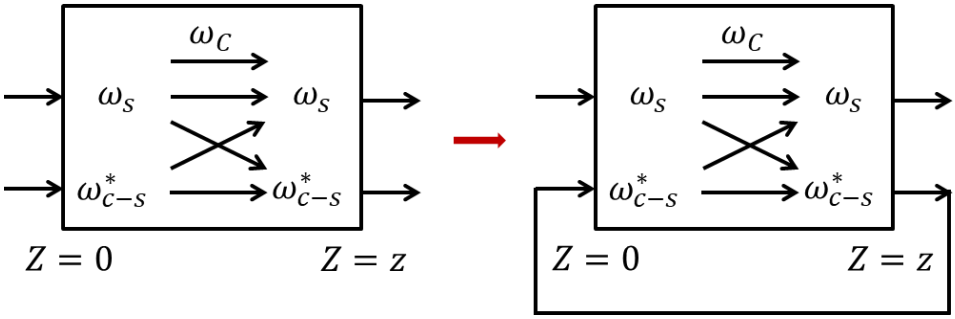

(a) (b)

Figure 3.3-1. (a)Symbol of TVTL showing the cross-coupling between ω_s and ω_{c-s} under the carrier drive at ω_c. (b)Symbol of TVTL with feedback from the output to input at ω_{c-s}.

$$\begin{bmatrix} V_s^-(z) \\ V_{c-s}^{*-}(z) \end{bmatrix} = \begin{pmatrix} t_{11} & t_{12} \\ t_{21} & t_{22} \end{pmatrix} \begin{bmatrix} V_s^+(0) \\ V_{c-s}^{*+}(0) \end{bmatrix} \tag{3.3-1}$$

In the four-wave mixing condition, the cross-coupling matrix could be expressed as Eq. (3.3-2).

$$\begin{cases} \mathrm{t}_{11} = \cos(\frac{1}{2\sqrt{2}}\xi\beta_s z)e^{-(\alpha_s+j\beta_s)z} \\ \mathrm{t}_{12} = \mathrm{j}\frac{1}{\sqrt{2}}\frac{\beta_s}{\beta_{c-s}}\sin(\frac{1}{2\sqrt{2}}\xi\beta_{c-s}z)e^{-(\alpha_s+j\beta_s)z} \\ \mathrm{t}_{21} = -\mathrm{j}\frac{1}{\sqrt{2}}\frac{\beta_{c-s}}{\beta_s}\sin(\frac{1}{2\sqrt{2}}\xi\beta_s z)e^{-(\alpha_{c-s}+j\beta_{c-s})z} \\ \mathrm{t}_{22} = \cos(\frac{1}{2\sqrt{2}}\xi\beta_{c-s}z)e^{-(\alpha_{c-s}-j\beta_{c-s})z} \end{cases} \quad (3.3\text{-}2)$$

In the three-wave mixing condition, the cross-coupling matrix could be expressed as Eq. (3.3-3).

$$\begin{cases} \mathrm{t}_{11} = \cosh(\frac{1}{4}\xi\sqrt{\beta_s\beta_{c-s}}z)e^{-(\alpha_s+j\beta_s)z} \\ \mathrm{t}_{12} = \mathrm{j}\sqrt{\frac{\beta_s}{\beta_{c-s}}}\sinh(\frac{1}{4}\xi\sqrt{\beta_s\beta_{c-s}}z)e^{-(\alpha_s+j\beta_s)z} \\ \mathrm{t}_{21} = -\mathrm{j}\sqrt{\frac{\beta_{c-s}}{\beta_s}}\sinh(\frac{1}{4}\xi\sqrt{\beta_s\beta_{c-s}}z)e^{-(\alpha_{c-s}+j\beta_{c-s})z} \\ \mathrm{t}_{22} = \cosh(\frac{1}{4}\xi\sqrt{\beta_s\beta_{c-s}}z)e^{-(\alpha_{c-s}-j\beta_{c-s})z} \end{cases} \quad (3.3\text{-}3)$$

If the output at ω_{c-s} is coupled back to the input to form a feedback loop in a way illustrated in Figure 3.3-1(b) and the condition that $V_{c-s}^{*-}(z) = V_{c-s}^{*+}(0)$ holds. Substituting this condition into Eq. (3.3-1) yields:

$$\begin{aligned} V_{c-s}^{*-}(z) &= t_{21}\cdot V_{c-s}^{*+}(z) + t_{22}\cdot V_{c-s}^{*+}(z) \\ &= t_{21}\cdot V_{c-s}^{*+}(z) + t_{22}\cdot V_{c-s}^{*-}(z) \end{aligned} \quad (3.3\text{-}4)$$

This leads to the following relationship:

$$\begin{cases} V_s^-(z) = t_{11} + \frac{t_{12}t_{21}}{1-t_{22}}V_s^+(0) = G_{s,s}V_s^+(0) \\ V_{c-s}^-(z) = \frac{t_{21}}{1-t_{22}}V_s^+(0) = G_{c-s,s}V_s^+(0) \end{cases} \quad (3.3\text{-}5)$$

Where $G_{s,s}$ is the voltage gain at the original signal frequency ω_s and $G_{c-s,s}$ is the cross frequency voltage gain between the output signal at the frequency of ω_{c-s} and the input signal at the frequency of ω_s. If the feedback path builds a resonance at the frequency of ω_{c-s} when the loop meets the condition of $\beta_{c-s}z = 2\pi$, thus, $1 - t_{22}$ is close to 0, a sharp rising gain would be

formed around the resonance for the lower side band of the upconverted signal. Usually, the resonance frequency of the loop is fixed and at ω_{c-s}. From Eq. (3.3-5), it is evident that a strong frequency selectivity at ω_{c-s} is coupled to the RF signal at ω_s, which forms a strong notch amplification that is tunable by controlling the carrier frequency. And conversion between the original frequency at ω_s and frequency at ω_{c-s} in Figure 3.3-1(b) behaves like a tunable filter but with a frequency shift.

3.3.2 Closed loop time-varying transmission line correlator

Initial simulation verification is carried out by using ADS HB simulation. The simulation schematic is shown in Figure 3.3-2. An extra amplifier and a coupler are inserted in the feedback loop for the purpose of changing the loop gain and sensing the converted band signal power separately. Two LC parallel resonators resonate at converted signal frequency are add at the port 1 and port 2 to trap the signal inside the loop.

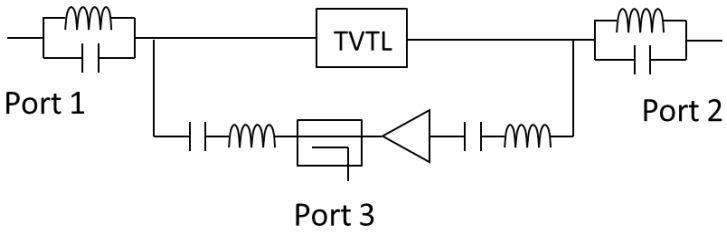

Figure 3.3-2. Schematic of the closed loop correlator.

Both carrier and signal are combined and fed through the port 1. At port 2, the converted signal is rejected and amplitude of the original signal is measured. At port 3, converted signal is sensed by a $3dB$ coupler. The feedback loop is intentionally tuned to be resonated at the

frequency of $3.5GHz$, when the carrier f_c is changing from the $4.3GHz - 4.7GHz$ with a step of $0.1GHz$ which corresponds to select input signal frequency of $f_c - 3.5GHz$.

Figure 3.3-3 shows the gain of the tunable filter. Greater than $20dB$ gain and off band suppression more than $35dB$ could be achieved. Figure 3.3-4 shows the gain of the tunable amplifier, a maximum gain of $15dB$ is reached. Bandwidth could be altered by tuning the gain of the inserted amplifier as shown in Figure 3.3-5, at the same time, the time constant of the loop changes correspondingly from $0.02\mu s - 0.1\mu s$.

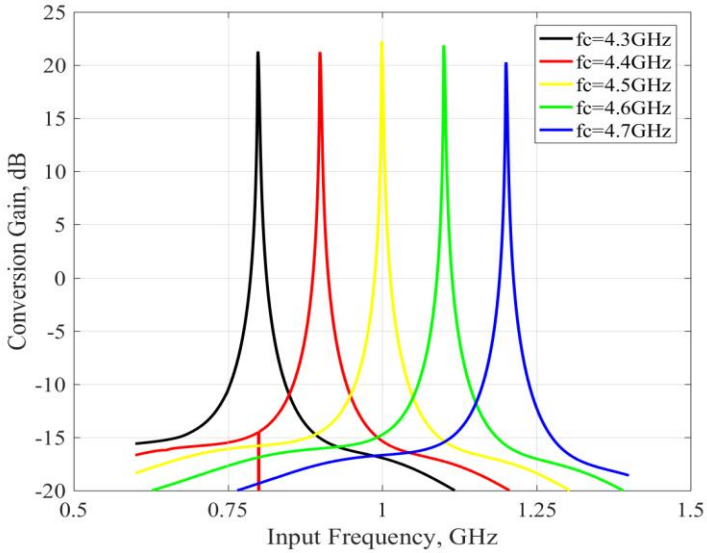

Figure 3.3-3. Conversion gain of the tunable filter while altering the carrier frequency.

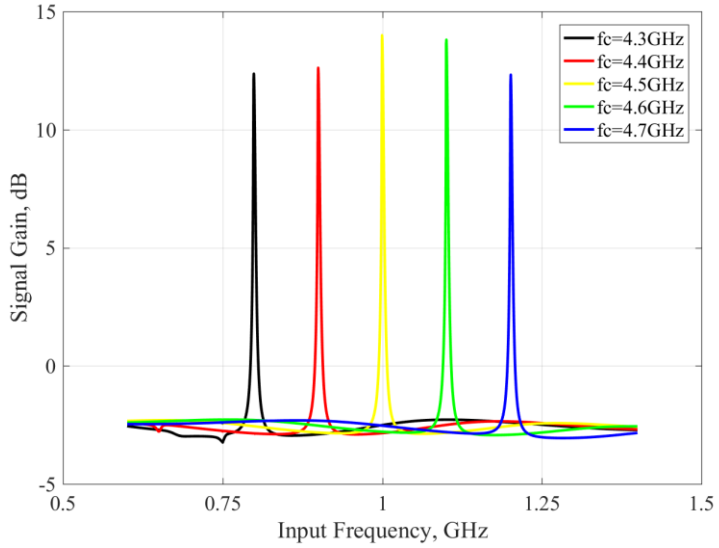

Figure 3.3-4. Signal gain of the tunable amplifier while altering the carrier frequency.

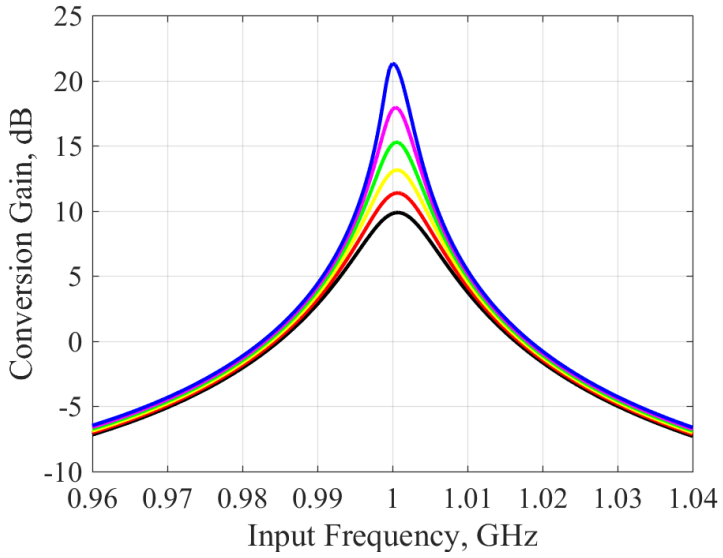

Figure 3.3-5. Conversion gain bandwidth versus the loop gain.

The high gain is reached when the loop gain close to 1. But in reality, instability and noise oscillation must be avoided.

The schematic of the implemented closed loop TVTL correlator is depicted in Figure 3.3-6. Both received signal and reference/carrier are combined by a triplexer and feed into the TVTL. Multiplication is realized by parametric mixing of the TVTL, a triplexer connected at the output of the TVTL to separate reference/carrier, original signal, and converted signal. Integration is performed by feeding back the converted signal into the input and correlation signal is extracted in the feedback loop through a coupler. Integration bandwidth and integration time constant can be controlled by changing the loop gain by an amplifier. The bandwidth of the correlator is sustainable through the whole TVTL bandwidth. Because of the extra amplifier and coupler inside the loop, the conversion gain could be revised as Eq. (3.3-6).

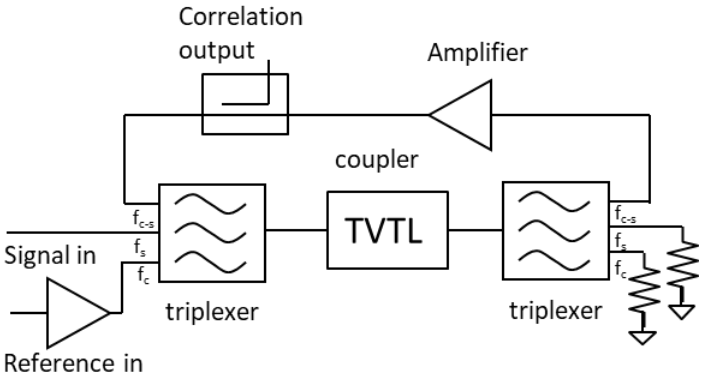

Figure 3.3-6. Schematic of the closed loop correlator.

$$G'_{c-s,s} = \frac{t_{21} \cdot G_a}{1 - G_{loop}} \cdot G_{co} \tag{3.3-6}$$

Where the $G_{loop} = t_{22} \cdot G_a \cdot G_l$ represents the loop gain which should be smaller than 1 to avoid oscillation. G_a denotes the gain of the amplifier, G_l and G_{co} are the insertion loss and coupling coefficient of the coupler.

Figure 3.3-7 gives the implemented closed loop correlator. MMIC coupler, an insertion loss of $2dB$ and a coupling coefficient of $6.5dB$, and amplifier are fabricated on the same InGaP HBT process as the TVTL fabrication. Triplexer is designed by cascading two diplexers which are designed by using the lumped components and microwave transmission lines.

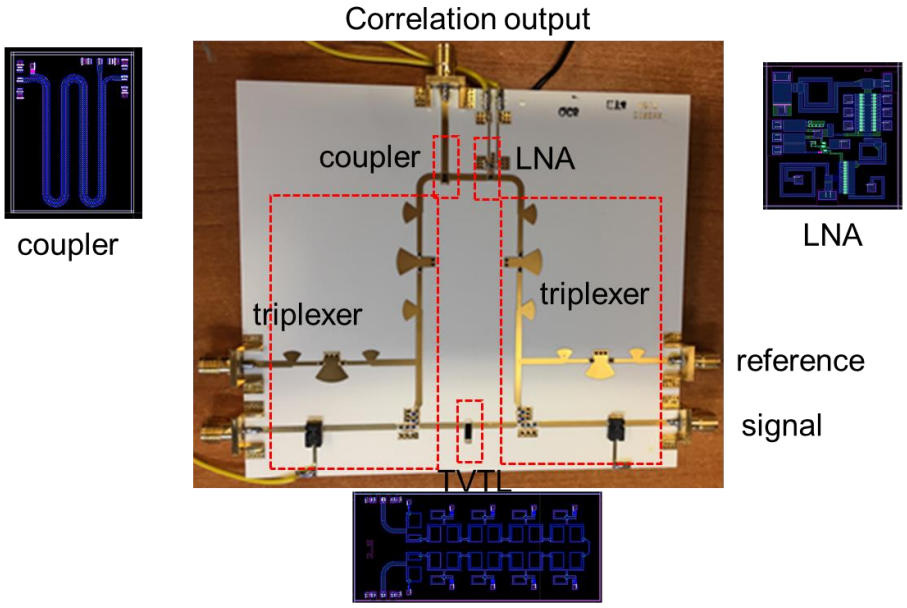

Figure 3.3-7. Implementation of the closed loop correlator.

The designed closed loop correlator operates at a four-wave mixing condition and resonates around at $\omega_{c-s} = 3.75GH$. Figure 3.3-8 shows conversion gain with different carrier frequencies tuned from $4.6GHz - 4.8GHz$. The maximum positive gain of $6dB$ is measured at the reference/carrier of $4.8GHz$ and close to $20dB$ suppression to the out of band signal. Figure 3.3-9 shows the conversion gain while changing the loop gain at the reference/carrier frequency of $4.8GHz$.

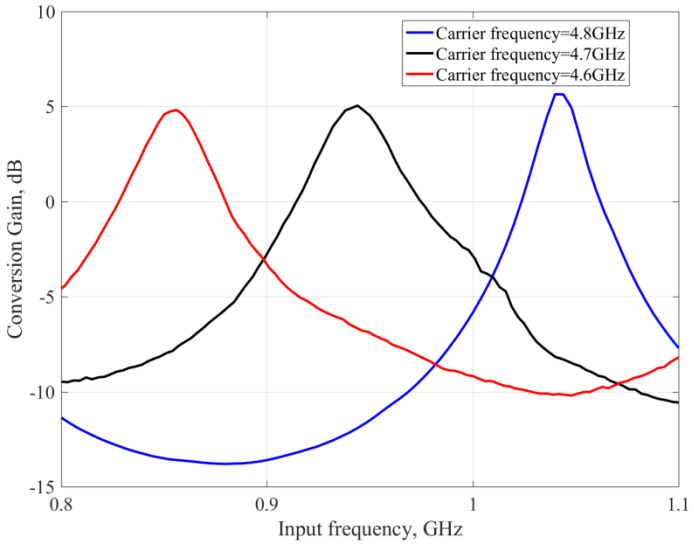

Figure 3.3-8. Measured conversion gain of the closed loop correlator with reference/carrier frequency tuned from $4.6GHz - 4.8GHz$.

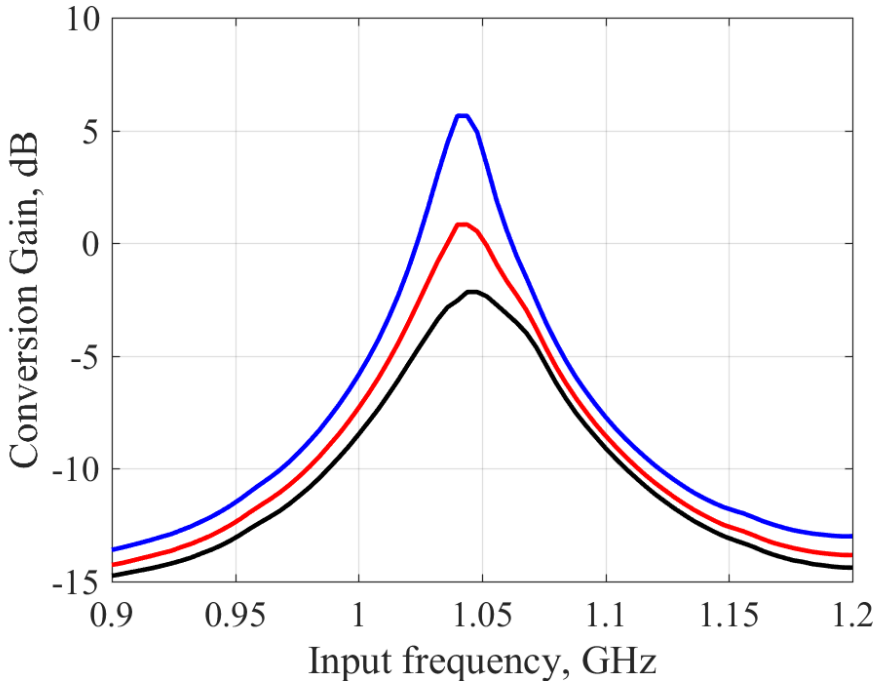

Figure 3.3-9. Measured conversion gain of the closed loop correlator with different loop gain at the reference/carrier frequency of $4.8GHz$.

3.3.3 Noise analysis of closed Loop time-varying transmission line correlator

There are multiple noise sources that would contribute to the total noise power at the output of the closed loop correlator and the noise factor calculation followed by first identifying each individual noise source and its transfer function, then calculating the total noise power at the output.

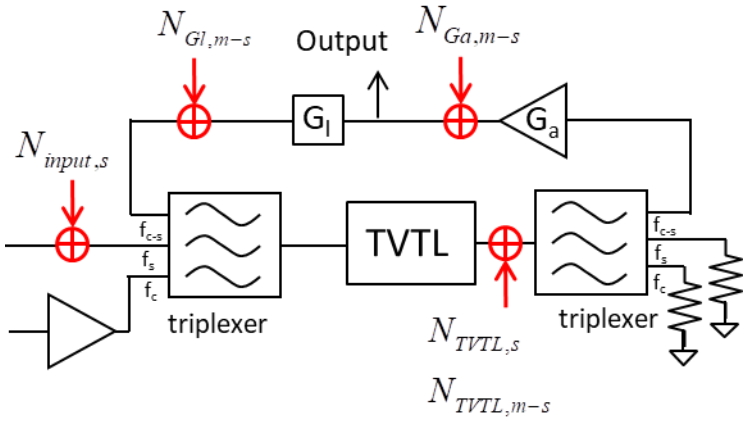

Figure 3.3-10. Noise source of the closed loop correlator.

Figure 3.3-10 shows the noise generated by each component and detailed discussions are followed:

Define Eq. (3.3-7) as the conversion gain from converted signal in the loop to the original signal.

$$G''_{C-S,S} = \frac{t_{21} \cdot G_a}{1 - G_{loop}} \tag{3.3-7}$$

A. Noise from the input termination: input 50Ω directly emits thermal noise into the loop which is converted to the converted band. Its transfer function to the output is the same as the signal cross frequency gain which leads to the output noise power:

$$N_{output,in} = KTB \cdot \left|G''_{c-s,s}\right|^2 \tag{3.3-8}$$

B. Noise from the TVTL can be decomposed into two parts, the first part is the noise from the signal band with equivalent noise power of $KTB \cdot \frac{1}{3}\frac{\beta_s z}{Q_s}$ and its transfer function is equal to $G''_{c-s,s}$, so the noise power contributed by the TVTL from the signal band is:

$$N_{output,s} = KTB \cdot \frac{1}{3}\frac{\beta_s z}{Q_s} \cdot \left|G''_{c-s,s}\right|^2 \tag{3.3-9}$$

C. The second part noise from the TVTL is from the converted band and it would be accumulated in the feedback loop. The transfer function with the equivalent noise source of $KTB \cdot \frac{1}{G_c^2}\frac{\beta_{c-s} z}{Q_{c-s}}$ is:

$$T_{output,c-s} = G''_{c-s,s} = \frac{t_{21} \cdot G_a}{1-G_{loop}} \tag{3.3-10}$$

Then the output noise power is:

$$N_{output,c-s} = KTB \cdot \frac{1}{G_c^2}\frac{\beta_{c-s} z}{Q_{c-s}} \cdot \left|G''_{c-s,s}\right|^2 \tag{3.3-11}$$

D. Noise power contributed by the amplifier with the voltage gain of G_a and noise factor of F_a. The transfer function of this noise to the output is:

$$T_{output,Ga} = \frac{G_a}{1-G_{loop}} \tag{3.3-12}$$

And the noise power at the output is:

$$N_{output,Ga} = KTB \cdot (F_a - 1) \cdot \left|T_{output,Ga}\right|^2 \tag{3.3-13}$$

D. Noise from the insertion loss from the coupler with the noise factor of $F_l = 1/G_l^2$ and its transfer function is:

$$T_{output,Gl} = \frac{t_{22} \cdot G_l \cdot G_a}{1 - G_{loop}} \tag{3.3-14}$$

And the noise power is:

$$N_{output,Gl} = KTB \cdot (F_l - 1) \cdot \left|T_{output,Gl}\right|^2 \tag{3.3-15}$$

The noise factor can be calculated by:

$$F_T = \frac{N_{output,in} + N_{output,s} + N_{output,c-s} + N_{output,Ga} + N_{output,Gl}}{KTB \cdot \left|G''_{c-s,s}\right|^2}$$

$$= 1 + \frac{1}{3}\frac{\beta_s z}{Q_s} + \frac{1}{G_c^2}\frac{\beta_{c-s} z}{Q_{c-s}} + \frac{(F_a - 1)}{|t_{21}|^2} + (F_l - 1) \cdot \left|\frac{t_{22} \cdot G_l}{t_{21}}\right|^2 \tag{3.3-16}$$

The converted signal inside the loop would be sensed through the coupler, which the final noise factor can be treated as two cascade stages, by applying Friis formulas for noise, the total noise factor of the closed loop correlator is:

$$F'_T = F_T + \frac{F_{co} - 1}{\left|G''_{c-s,s}\right|^2} \tag{3.3-17}$$

Where $F_{co} = 1/|G_{co}|^2$ is the coupler's noise factor at the coupling port.

Figure 3.3-11 shows the conversion gain/noise figure versus the loop gain G_{loop} from $0.5 - 1.0$, which indicates as the loop gain increases, the noise figure would be decreasing accordingly. But as the loop gain getting close to 1, the circuit could be potentially unstable.

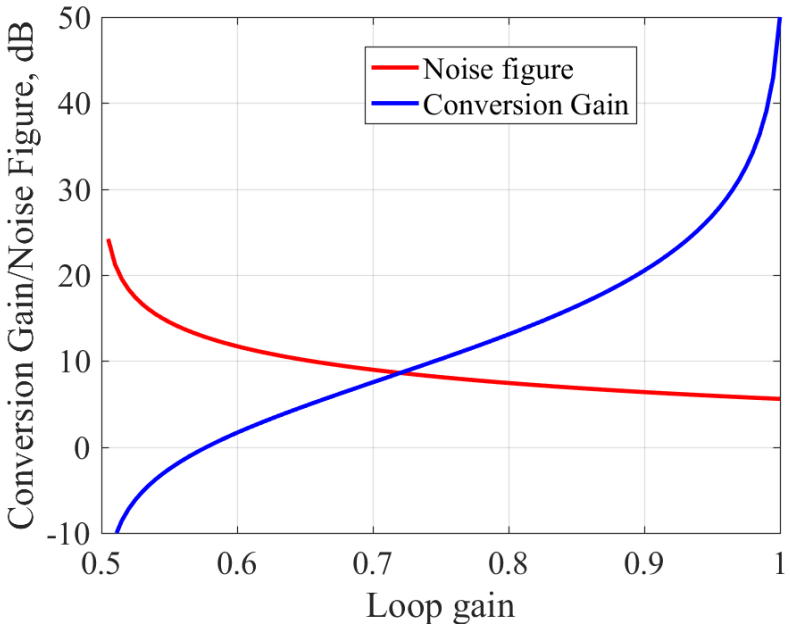

Figure 3.3-11. Conversion gain/noise figure versus the loop gain of the closed loop correlator.

Figure 3.3-12 shows the measured, simulated and theoretical noise figure under the conversion gain equals to $-3dB$ and the minimum noise figure of $13dB$ is achieved.

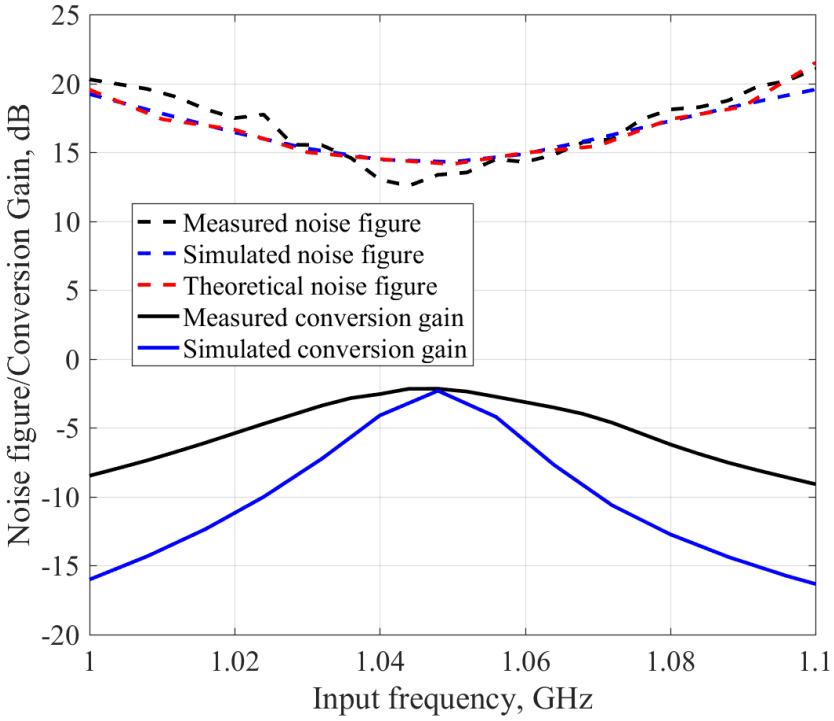

Figure 3.3-12. The measured, simulated and theoretical noise figure of the closed loop correlator at the reference/carrier frequency of $4.8GHz$.

By comparing these two TVTL based open loop and closed loop correlator, open loop one usually has a better noise figure and closed loop correlator could achieve a much higher conversion gain with build-in integration achieved by the feedback loop without needing an extra filter. However, the loop gain of the closed loop correlator should be smaller than 1 to avoid self-oscillation.

Chapter 4

Advanced Time-varying Transmission Line (TVTL) Structures

Fundamentally, the TVTL should not consume any carrier power except the power that converted to the converted bands. However, all previously designed traveling-wave TVTLs dumped part of the carrier power on the 50Ω termination at the output and lossy transmission line. By using the advanced TVTL structures, the carrier directly modulates the varactor diodes, which saves carrier power and improves power efficiency. Meanwhile, in the new structure, extra combiner for combining carrier and signal is not needed anymore.

4.1 Direct-pumped Time-varying Transmission Line

Figure 4.1-1 shows the schematic of the direct-pumped TVTL. Both signal and carrier propagate in a differential fashion. On the carrier path, the carrier is split by a 90-degree hybrid and then differentiated by a balun to create the matched phase that emulates the traveling wave propagation on the TVTL. The carrier is directly fed onto the varactor diodes so that no power wasted on 50Ω termination and transmission line. On the signal path, the signal is fed into the input port then differentiated by a balun. At the output, a diplexer is connected for the purpose of terminating the original signal and separating the upconverted signal. Since the virtual ground created on the diode bridge by the using the differential signals, no power leakage between the signal path and the carrier path. Furthermore, the carrier frequency could be located at the cutoff frequency of the TVTL, which could easily enable the three-way mixing and let upper sideband converted signal falls into the stopband of the TVTL. At the same time, the carrier modulates

each varactor with the same amplitude, unlike the traveling wave that the amplitude of which would decay along on the transmission line.

The designed chip is fabricated by Global Communication Semiconductors (GCS) InGaP HBT process. Figure 4.1-2 shows the layout of the fabricated TVTL chip. The size of this designed direct-pumped TVTL is $10150\mu m \cdot 6393\mu m$. Signal in and out are located at the left and right sides of the chip, the carrier is split by an extra 90-degree hybrid and fed into the upper and lower sides of the chip.

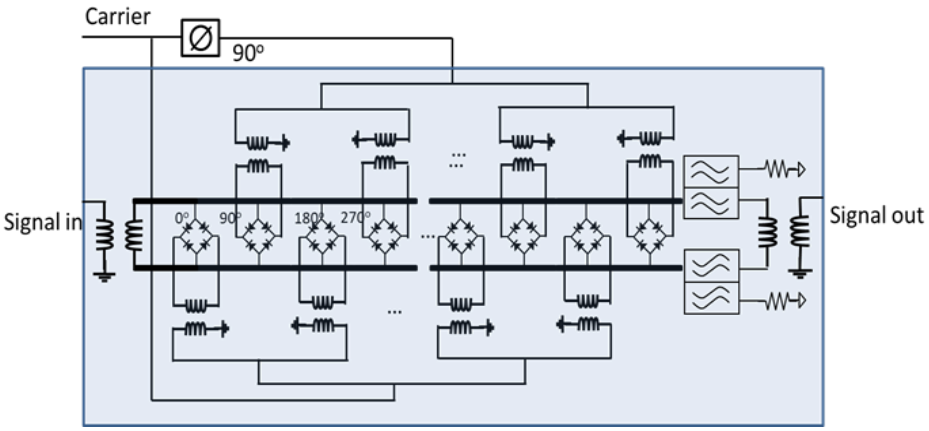

Figure 4.1-1. Schematic of the direct-pumped TVTL.

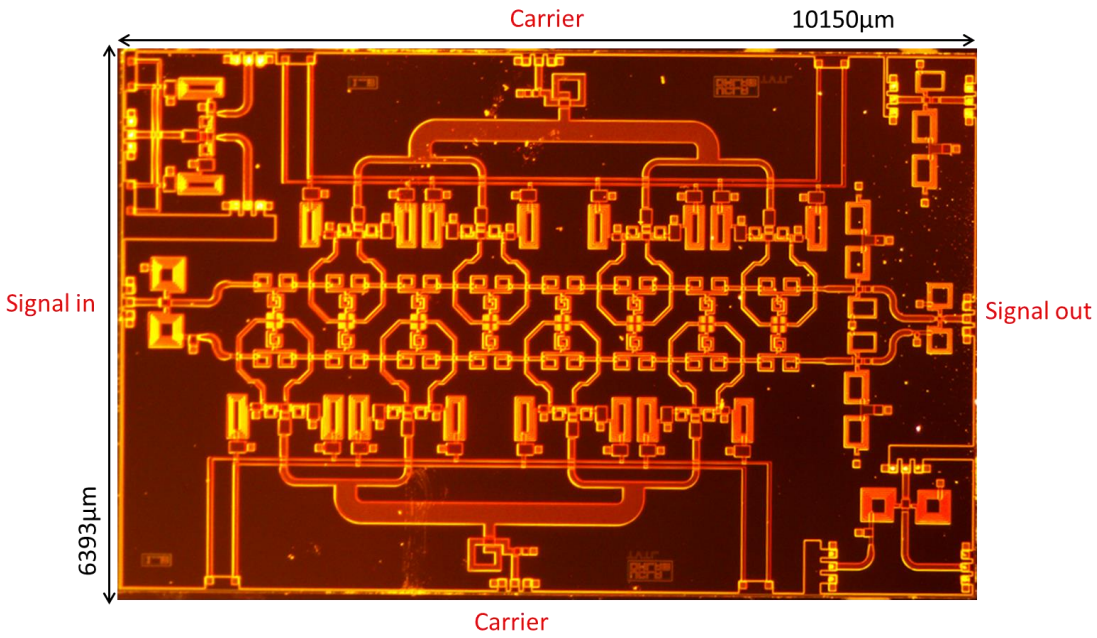

Figure 4.1-2. Layout of the direct-pumped TVTL.

In Figure 4.1-3, the solid black line is the measured lower sideband conversion gain around $0dB$ is achieved under the varactor biased at $-4V$, input signal frequency is from $0.5GHz - 1.5GHz$ with the power of $-10dBm$ and carrier frequency at $5GHz$ with the power of $30dBm$. In the practical implementation, in order to split and differentiate the carrier and signal, extra LC-based narrow band baluns and T-junction splitters are needed which could introduce additional loss approximately equal to $5dB$. Theoretical and simulated results are plotted for comparison in Figure 4.1-3. The theoretical conversion gain is predicted by Eq. (2.1-10), three-wave mixing condition, with extra propagation, baluns, and diplexer losses added.

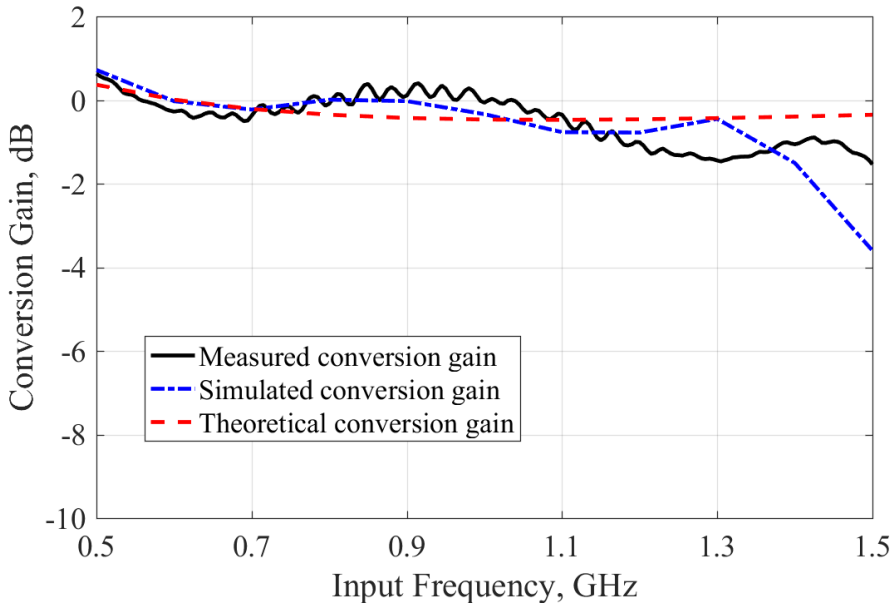

Figure 4.1-3. Conversion gain of the designed direct-pumped TVTL with varactor biased at $-4V$, carrier power of $30dBm$ at $5.0GHz$.

Figure 4.1-4 shows the noise figure results of the direct-pumped TVTL. The theoretical noise figure is derived by first calculating the noise figure of TVTL structure in the middle of Figure 4.1-1 and then using Friis formulas for the entire cascade stages by knowing the losses from the diplexers and baluns. The measured noise figure signal frequency is from $0.995GHz - 1.003GHz$, an average of $4.5dB$ noise figure is achieved and good matching among the measurement, simulation, and theory is shown. The input referred $P1dB$ of this TVTL is $16dBm$, as shown in Figure 4.1-5.

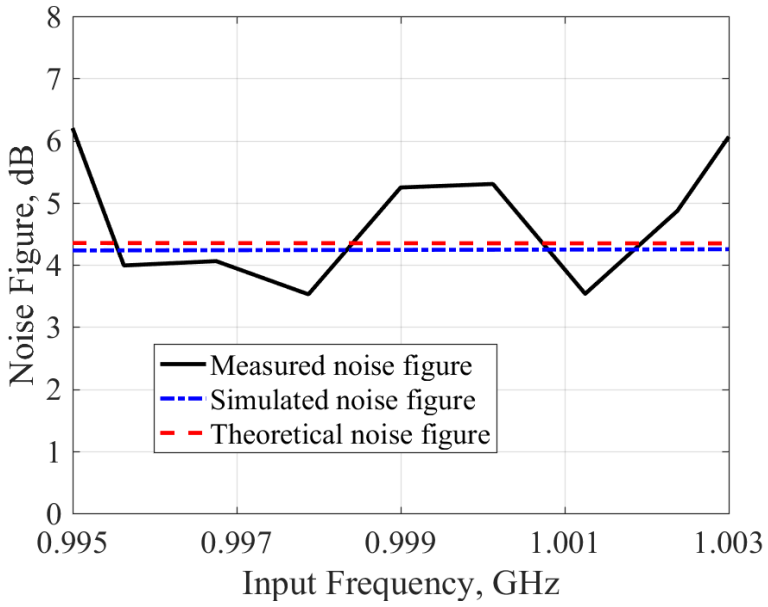

Figure 4.1-4. Noise figure of the designed direct-pumped TVTL with varactor biased at $-4V$, carrier power of $30dBm$ at $5.0GHz$.

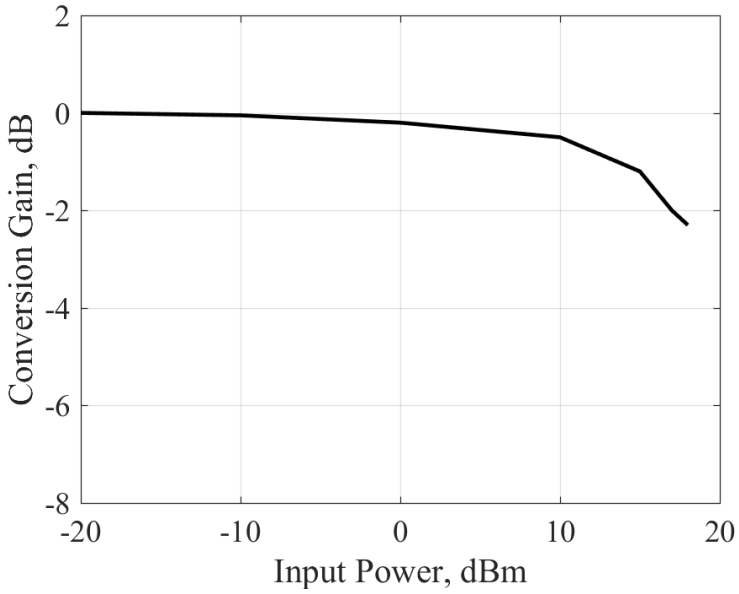

Figure 4.1-5. Measured conversion gain of the direct-pumped TVTL versus input power with varactor biased at $-4V$, carrier power of $30dBm$ at $5.0GHz$.

4.2 Reflected Time-varying Transmission Line

Figure 4.2-1 shows the schematic of a different TVTL design that offers power effective frequency conversion. At the output, compared with the direct-pumped TVTL, the diplexer is replaced by a highpass filter which passes the converted signal but reflects the original signal. At the input of the TVTL, a matching circuit is designed to recycle the reflected original signal so that a much higher conversion gain could be reached. But the bandwidth of the circuit is sacrificed because of the resonance or standing wave created between the highpass filter at the output and the matching circuit at the input.

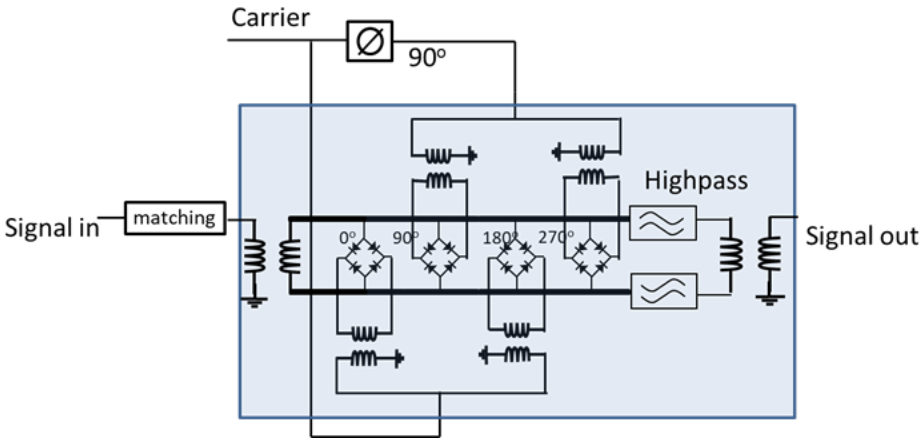

Figure 4.2-1. Schematic of the reflected TVTL.

The overall voltage conversion gain G_c^r could be found by [34]:

$$G_c^r = \frac{\sqrt{1-|S_{11}|^2}}{1-|S_{11}|\sqrt{G_s}e^{j(\phi_T+\phi_M)}} G_c \tag{4.2-1}$$

Where S_{11} is the return loss of the input matching circuit under the 50Ω termination, G_s is the signal gain as indicated in Eq. (2.1-11), G_c is the original conversion gain as indicated in Eq.

(2.1-10) and $\phi_T + \phi_M$ is the phase delay of the converted signal. At the resonance condition, the phase term in the denominator of Eq. (4.2-1) disappears which results in the maximum conversion gain,

$$G_{c,max}^{r} = \frac{\sqrt{1-|S_{11}|^2}}{1-|S_{11}|\sqrt{G_s}} G_c \tag{4.2-2}$$

The noise figure of the reflected TVTL is given by Eq. (4.2-3).

$$NF = 1 + \frac{1}{3}\frac{\beta_s z}{Q_s} \cdot \frac{1}{1-|S_{11}|^2} + \frac{1}{G_c^{r2}} \cdot \frac{\beta_{c-s} z}{Q_{c-s}} \tag{4.2-3}$$

Figure 4.2-2 shows the fabricated reflected TVTL chip by using Global Communication Semiconductors (GCS) InGaP HBT process. The size of this designed reflected TVTL is $6393\mu m \cdot 5850\mu m$. An extra matching circuit is connected at the input, left side of the chip, of the chip, the output is on the right side of the chip. Carrier is split by a 90-degree hybrid and fed into the upper and lower sides of the chip.

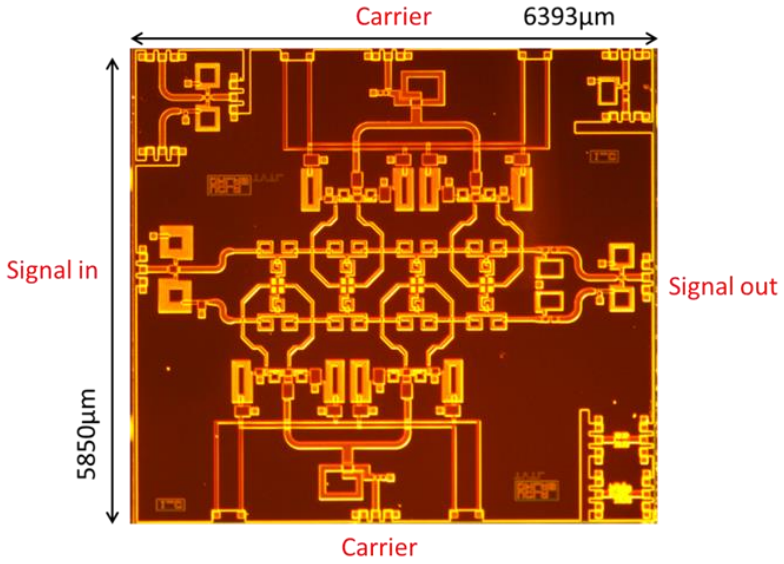

Figure 4.2-2. Layout of the reflected TVTL.

The conversion gain is shown in Figure 4.2-3 with a signal from $0.7GHz - 1.3GHz$, carrier of $4.8GHz$ with power of $27dBm$, a maximum gain of $4dB$ can be obtained but with a narrow bandwidth. The noise figure is also measured, simulated, and calculated by theory, the results are shown in Figure 4.2-4, and a minimum of $4.5dB$ is achieved. Because of the standing wave created on the TVTL, at least of $6dB$ decreasing compared with direct-pumped TVTL's $P1dB$ should be expected. Figure 4.2-5 shows the result of the input referred $P1dB$, $8dBm$ could be reached.

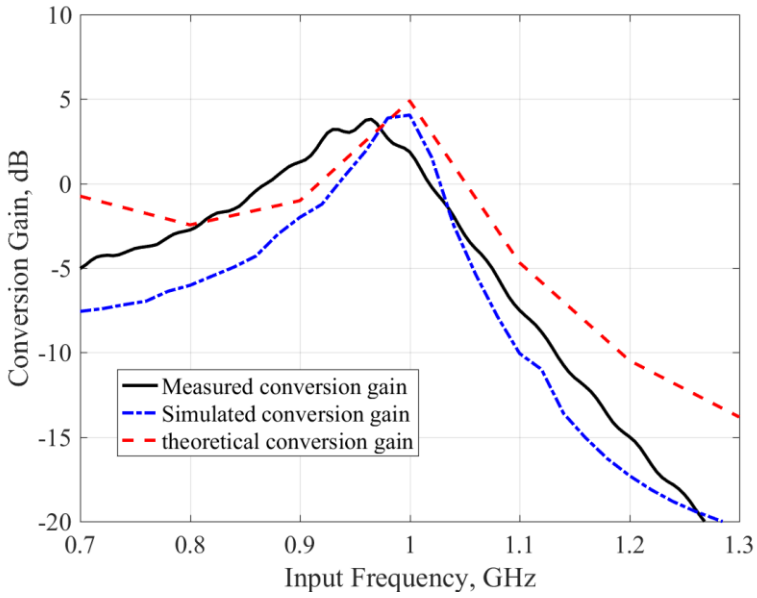

Figure 4.2-3. Conversion gain of the designed reflected TVTL with varactor biased at $-4V$, carrier power of $27dBm$ at $4.8GHz$.

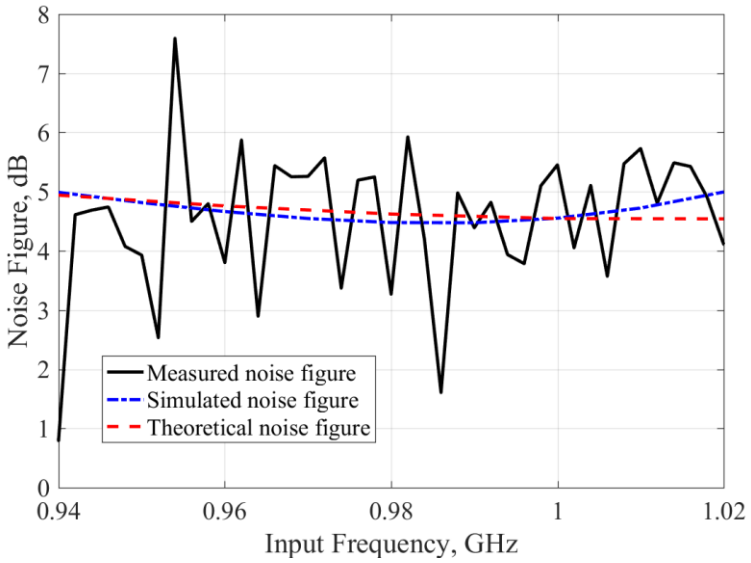

Figure 4.2-4. Noise figure of the designed reflected TVTL with varactor biased at $-4V$, carrier power of $27dBm$ at $4.8GHz$.

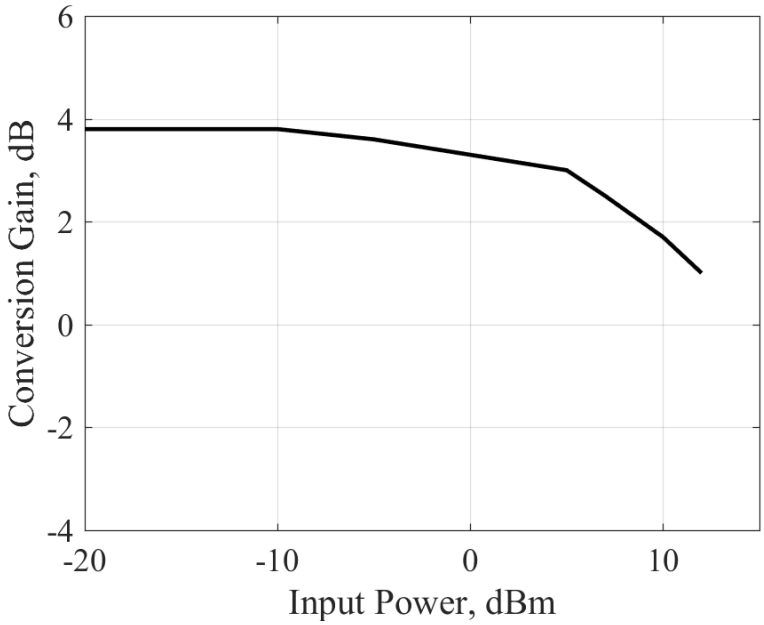

Figure 4.2-5. Measured conversion gain of the reflected TVTL versus input power with varactor biased at $-4V$, carrier power of $27dBm$ at $4.8GHz$.

Chapter 4

Conclusion

In this work, two time-varying transmission line (TVTL) based RF correlators, open loop and closed loop correlators, are successfully proposed, designed and fabricated, which could find applications in RF wireless system to reject in-band jammer and interference by using orthogonal codes.

Basic TVTL structure is explored, inductor pumped structure and M-derived TVTL are proposed for the purpose of decreasing the chip area and improving power efficiency. MMIC version M-derived TVTL chip is designed and fabricated with Global Communication Semiconductors (GCS) InGaP HBT process, both simulation and measurement are tested under the four-wave mixing condition and three-wave mixing condition.

An open loop correlator is designed, where the multiplication is fulfilled by the parametric mixing of the TVTL and integration is realized by a high-Q bandpass filter. The design illustrates low loss, low noise and high power handling capability of the TVTL based correlator. Frequency domain correlation test and time domain decoder test are also carried out. Another TVTL based closed loop correlator is designed, which the integration is finished by the feedback loop. The design shows a higher conversion gain but worse noise performance.

Moreover, two advanced TVTL structures are proposed. The carrier power is directly pumped on the varactors to save the energy wasted on the transmission line and 50Ω load that happens in the traveling TVTL case.

Finally, all TVTL designs employ numerous inductors with limited quality factor (Q) which introduce a significant amount of loss and noise, so new inductor structure or more advanced process with low loss still needs to be explored and applied. TVTL is usually the very broadband device, the power efficiency or conversion gain could be possibly improved by trading off the bandwidth.

References

[1] Haykin, Simon, Communication systems, 2015.

[2] D. Torriei, Principle of spread-spectrum communication systems, 4th ed, 2018.

[3] S. Qin, Q. Xu, and Y. E. Wang, "Nonreciprocal components with distributedly modulated capacitors," *IEEE Trans. Microw. Theory Techn.*, vol. 62, no. 10, p. 2260–2272, Oct. 2014.

[4] M. Biedka, Q. Wu, X. Zou, S. Qin and Y. E. Wang, "Integrated time-varying electromagnetic devices for ultra-wide band nonreciprocity," in *IEEE Radio Wireless Symp. (RWS)*, Anaheim, CA, USA, Jan. 2018.

[5] Y. E. Wang, "Non-reciprocity with time-varying transmisison lines (TVTLs)," in *IEEE Int. Wireless Inform. Technol. Syst. Conf*, Maui, Hi, USA, Nov. 2012.

[6] X. Zou, Q. Wu, and Y.E. Wang, "Monolithically Integrated Parametric Mixers with Time-varying Transmission Lines (TVTL)," *IEEE MTT-S International Microwave Symposium (IMS)*, Jun. 2019.

[7] S. Qin, and Y. E. Wang, "Parametric conversion with distributedly modulated capacitors (DMC) for low-noise and non-reciprocal RF front-ends," in *IEEE MTT-S Int. Microw. Symp. Dig.*, Seattle, WA, USA, Jun. 2013.

[8] Y. E. Wang, "Time-varying transmission lines (TVTL) - A new pathway to nonreciprocal and intelligent RF front-ends," in *Proc. IEEE Radio Wireless Symp.* , Newport Beach, CA,

USA, Jan. 2014.

[9] Q. Wu, X. Zou, S. Qin and Y. E. Wang, "Frequency translational RF receiver with time-varying transmission lines," in *IEEE MTT-S International Microwave Symposium (IMS)*, Honolulu, HI, USA, Jun. 2017.

[10] Y. Li, X, Yu, and Z, Lu, "Nonreciprocal time-varying transmission line with carrier boosting technique for low-noise RF front ends," *IEEE Microw. Wireless Components Letters* , vol. 28, no. 11, pp. 1011-1013, Nov. 2018.

[11] Q. Wu, X. Zou, R. Zhu and Y. E. Wang, "Chip-Scale RF correlator with monolithically integrated Time-varying Transmission Line (TVTL)," in *IEEE MTT-S International Microwave Symposium (IMS)*, Philadelphia, Jun. 2018.

[12] C. Andrews, A. C. Molnar, "A passive mixer-first receiver with digitally controlled and widely tunable RF interface," *IEEE Journ. Solid-State Cirt.*, vol. 45, no. 12, pp. 2696-2708, Dec. 2010.

[13] Y. Lien, E. Klumperink, B. Tenbroek, J. Strange, B. Nauta, "A high-linearity CMOS receiver achieving +44dBm IIP3 and +13dBm B1dB for SAW-less LTE radio," *IEEE Intern. Solid-State Cirt. Conf.*, Feb. 2017.

[14] C. Luo, P. S. Gudem, and J. F. Buckwalter, "A 0.4–6-GHz 17-dBm B1dB 36-dBm IIP3 Channel-Selecting Low-Noise amplifier for SAW-Less 3G/4G FDD diversity receivers," *IEEE Trans. Micro. Theory and Techn.*, vol. 64, no. 4, pp. 1110-1211, Apr. 2016.

[15] D. Murphy, H. Darabi, A. Abidi, A. A. Hafez, A Mirzaei, M, Mikhemar, F. Chang, "A

Blocker-Tolerant, Noise-Cancelling Receiver Suitable for Wideband Wireless Applications," *IEEE Jour. Solid-State Circ.*, vol. 47, no. 12, pp. 2943-2963, Dec. 2012.

[16] A. Nejdel, M. Abdulaziz, M. Törmänen, and H. Sjöland, "A positive feedback passive mixer-first receiver front-end," *IEEE Radio Freq. Integ. Circ. Symp.*, May. 2015.

[17] Y. Lien, E. K. Klumperink, B. Tenbroek, J. Strange, and B. Nauta, "A mixer-first receiver with enhanced selectivity by capacitive positive feedback achieving +39dBm IIP3 and <3dB noise figure for SAW-less LTE Radio," *IEEE Radio Freq. Integ. Circ. Symp.*, June 2016.

[18] Troy, "Signal Processing at RF (SPAR)," 2016. [Online]. Available: https://www.darpa.mil/attachments/SignalProcessingRF_FINALforPosting.pdf.

[19] S. Qin, and Y. E. Wang, "Broadband parametric circulator with balanced monolithic integrated distributedly modulated capacitors (DMC)," in *IEEE MTT-S Int. Microw. Symp. Dig.*, San Francisco, CA, USA, May. 2016.

[20] S. Qin, "Broadband Nonreciprocal RF Front-Ends Based on Time-Varying Transmission Lines," UCLA Electronic Theses and Dissertations, 2016.

[21] Q. Wu, X. Zou, and Y. E. Wang, "Jamming resilient spread spectrum receiver with time-varying transmission line (TVTL) RF correlator," in *IEEE Radio and Wireless Symp.(accepted)*, San Antonio, Texas, USA, Jan. 2020.

[22] P P. K. Tien, "Parametric amplification and frequency mixing in propagating circuits," *J. Appl. Phys*, vol. 29, no. 9, p. 1347–1357, Sept. 1958.

[23] P. K. Tien, and H. Suhl, "A traveling-wave ferromagnetic amplifier," *Proc. IEEE,* vol. 46, no. 4, pp. 700-706, Apr. 1958.

[24] A. Cullen, "A travelling-wave parametric amplifier," *Nature,* vol. 181, pp. 332-332, Apr. 1958.

[25] R. Landauer, "Parametric amplification and frequency mixing in propagating circuits," *J. Appl. Phys,* vol. 31, no. 3, pp. 479-484, Mar. 1960.

[26] D. Jager, and F. J. Tegude, "Nonlinear wave propagation along periodic-loaded transmission line," *J. Appl. Phys,* vol. 15, no. 4, pp. 393-397, Apr. 1978.

[27] B. Gray, B. Melville, and J. S. Kenney, "Analytical modeling of microwave parametric upconverters," *IEEE Trans. Microw. Theory Techn,* vol. 58, no. 8, Aug. 2010.

[28] S. Magierowski, J. F. Bousquet, Z. Zhao, and T. Zourntos, "RF CMOS parametric downconverters," *IEEE Trans. Microw. Theory Techn,* vol. 58, no. 3, pp. 518-528, Mar. 2010.

[29] A. Kamal, J. Clarke, and M. H. Devoret, "Noiseless non-reciprocity in a parametric active device," *Nature Phys,* vol. 7, pp. 311-315, Apr. 2011.

[30] R H Freeman and A E Karbowiak, "An investigation of nonlinear transmission lines and shock waves," *J. Phys,* vol. 10, pp. v53-65, 1977.

[31] E. Afshari, and A. Hajimiri, "Nonlinear Transmission Lines for Pulse Shaping in Sliicon," *IEEE journ. solid-state circuits,* vol. 40, no. 3, pp. 744-752, 2005.

[32] X. Zou, Q. Wu, and Y. E. Wang, "Parametrically enhanced delay line with monolithically integrated time-varying transmission lines (TVTL)," in *IEEE Radio and Wireless Symp.*, Orlando, FL, USA, Jan. 2019.

[33] David M Pozar, Microwave Engineering 4th, John Wiley & Sons, 2012.

[34] S. Qin, and Y. E. Wang, "A nonreciprocal, frequency-tunable notch amplifier based on distributedly modulated capacitors (DMC)," in *IEEE MTT-S Int. Mircow. Symp.* , San Francisco, CA, USA, May. 2016.

[35] X. Zou, Q. Wu, and Y. E. Wang, "Monolithically integrated parametric mixers with time-varying transmission lines (TVTL)," *IEEE MTT-S Trans. Microw. Theory and Techn.*, Submitted.